A CABLE-STAYED GEOMETRIC NONLINEAR ANALYSIS

by

David K. Delaney
Graduate Student in Civil Engineering
University of Alaska Fairbanks
Fairbanks, Alaska 99775

and

J. Leroy Hulsey
Associate Professor of Civil Engineering
University of Alaska Fairbanks
Fairbanks, Alaska 99775

December 1990

Report No. INE/TRC 90.01

TRANSPORTATION RESEARCH CENTER
INSTITUTE OF NORTHERN ENGINEERING
SCHOOL OF ENGINEERING
UNIVERSITY OF ALASKA FAIRBANKS
FAIRBANKS, ALASKA 99775

DISCLAIMER

This research has been funded by the Department of Civil Engineering at the University of Alaska Fairbanks. The contents of this report reflect the views of the authors, who are responsible for the facts and the accuracy of the data presented herein. The contents of the report do not necessarily reflect the views or policies of the sponsoring party. This work does not constitute a standard, specification, or regulation.

ABSTRACT

An element for modeling cable geometric nonlinearities of cable-stayed structures is developed. The three–node axial element can approximate cable deformed geometry and effective stiffness for use with the finite element method of analysis. Cable displacements are restricted to a single vertical plane and both transverse and axial displacements are accounted for. The element was integrated with a space frame finite element program and used in the three–dimensional nonlinear analysis of a cable–stayed bridge. Results were compared with experimental data. The correlation between computed and measured values was found to be very good. It was found that cable geometric nonlinearities did not significantly effect the bridge behavior because of high cable post–tensioning forces.

Table of Contents

Table of Contents Continued

List of Figures

List of Figures Continued

List of Tables

Acknowledgments

The authors would like to acknowledge the advice and criticism of Dr. Kevin Curtis and Dr. Jonah Lee. The authors also acknowledge Design Alaska, Inc. for their generosity in providing use of their computer facilities during the final stage of the work.

The authors would like to acknowledge the Alaska Department of Transportation and Public Facilities (AKDOT&PF) for providing an awarness to this problem.

1. INTRODUCTION

1.1 Research Objective

A cable–stayed structure usually consists of members supported by inclined ropes, cables, or chains connected to a mast or tower which extends above the structure from a support location. The idea is to facilitate longer spans of members where intermediate supports are either not feasible or not desired and beam depths become impractical. Basic elements of these structures have been used for centuries dating back to the Egyptians who applied the concept to their sailing ships. The concept was applied in tropical regions of the world to primitive types of foot bridges using vines attached to trees on either bank to support a walk of vines and bamboo sticks (Trotski(1988)).

Structural systems relying entirely or partially on cables for support may be characterized by behavior that is highly nonlinear depending on cable weight, initial tension, and orientation. When inclined cables are involved, members connected to cable ends can experience large compressive forces and deflections (e.g.; tower and girders). Members subjected to compressive axial loads and/or moments experience a phenomenon known as the P–Delta effect and these members can become unstable as the transverse deflections begin to increase nonlinearly with an increase in the compressive stress. The cables themselves, if not vertically oriented, can experience large deflections (drape) which increase or decrease nonlinearly with cable tension. This drape, which results from uniform distributed loads, body forces or a combination thereof, greatly affects the structural behavior of the system. These nonlinearities associated with structure geometry fall under the category of geometric nonlinearities and are present in a cable–stayed system. This investigation concentrated on the geometric nonlinearities associated with cables of a cable–stayed bridge.

In a cable–stayed bridge, the cables are usually post–tensioned to some predetermined state of stress. Several reasons for this are to:

1. Decrease girder dead load deflections;

2. Dampen dynamic motion of bridge deck; and

3. Stiffen the structure by reducing cable drape.

Unlike many flexible structures, cable stayed bridges tend to become stiffer as the stayed members deflect, that is, increments in load tend to result in consistently smaller increments in displacement. This is primarily because as cable tension increases the drape decreases and its behavior approaches that of an axial truss member. The smaller a cable's drape the more force required to displace its end axially, therefore, the stiffer the cable appears to the rest of the structure. Thus, initial cable tensions (cable post–tensioning force) existing before the structure is loaded can have a very important effect in the analysis of cable–stayed bridges.

When performing a static analysis of a cable–stayed bridge, nonlinear behavior due to the cables can present interesting and usually complex problems. Different analytical analysis techniques may be best suited for a particular structure type or configuration, and selection of the appropriate method to use for a cable–stayed bridge depends upon the assumptions made and the variables to be investigated. Pertinent questions the investigator should ask are: a) To what extent do cable geometric nonlinearities influence the state of stress of the system?; b) Are assumptions common to a two–dimensional analysis valid for this type of a structure?; c) Is a three–dimensional analysis necessary to gain an understanding of how the structure will behave?; d) How is the load distributed, and is the distribution effected by these nonlinearities?; e) What loading conditions should be examined and what is the appropriate method of applying these loads for the type of analysis performed?; and f) With the cables being post–tensioned, can their behavior be sufficiently approximated by linear elastic assumptions? It was the objective of this research to:

1. Develop a cable element to account for cable geometric nonlinearity in a finite element analysis;

2. Perform a 3–D analysis including cable nonlinearity on the Captain William Cooper Moore Creek Bridge for six load cases reproducing conditions tested in a previous experimental study (Hulsey et al.(1990)); and
3. Compare the 3–D results with a 2–D linear analysis and experimental data.

An element for modeling geometric nonlinear behavior of cable–stays was developed and used in a three–dimensional finite element analysis of the bridge. Details of element development, bridge model, and analysis performed are discussed in sections to follow.

1.2 Bridge Overview

The Captain William Cooper Moore Creek Bridge, located on the highway between Skagway, Alaska and Carcross, Canada, is an unusual cable–stayed bridge. The bridge consists of a 7–inch laminated timber plank deck supported by transverse floor beams spanning between two stiffened steel box–shaped girders. Shear plates were used for connecting floor beams to the girders. These connectors provide some degree of rotational resistance between the members. The girders are supported by column arrangements on their ends and are stayed at approximately mid–span by cable pairs in a double plane arrangement. The bridge has an overall length of 300 ft. which is divided over four span lengths of 30–123–127–20 ft. (see Figure 1.1)

The two main box–shaped girders were fabricated, in 60 ft. long sections, from steel plates welded at the corners. These 60 ft. sections were spliced together at the ends with plates bolted inside and outside the box. The original overall dimensions of the girders were 2 ft. 6–5/8 inches by 5 ft. 1 inch. Each girder is stayed at approximately mid–span by two 3 inch diameter inclined cables constructed of galvanized structural strands. The cables extend through the girders and are anchored to the underside of the bottom flange. The stays are supported above the deck by an inclined H–shaped tower which has two transverse beams near its top. The tower is supported by the canyon's rock wall at the base, extends up to and supports the girders, and continues up approximately 106 ft. with a tapered box–shaped cross–section. The steel tower is inclined forward over the canyon

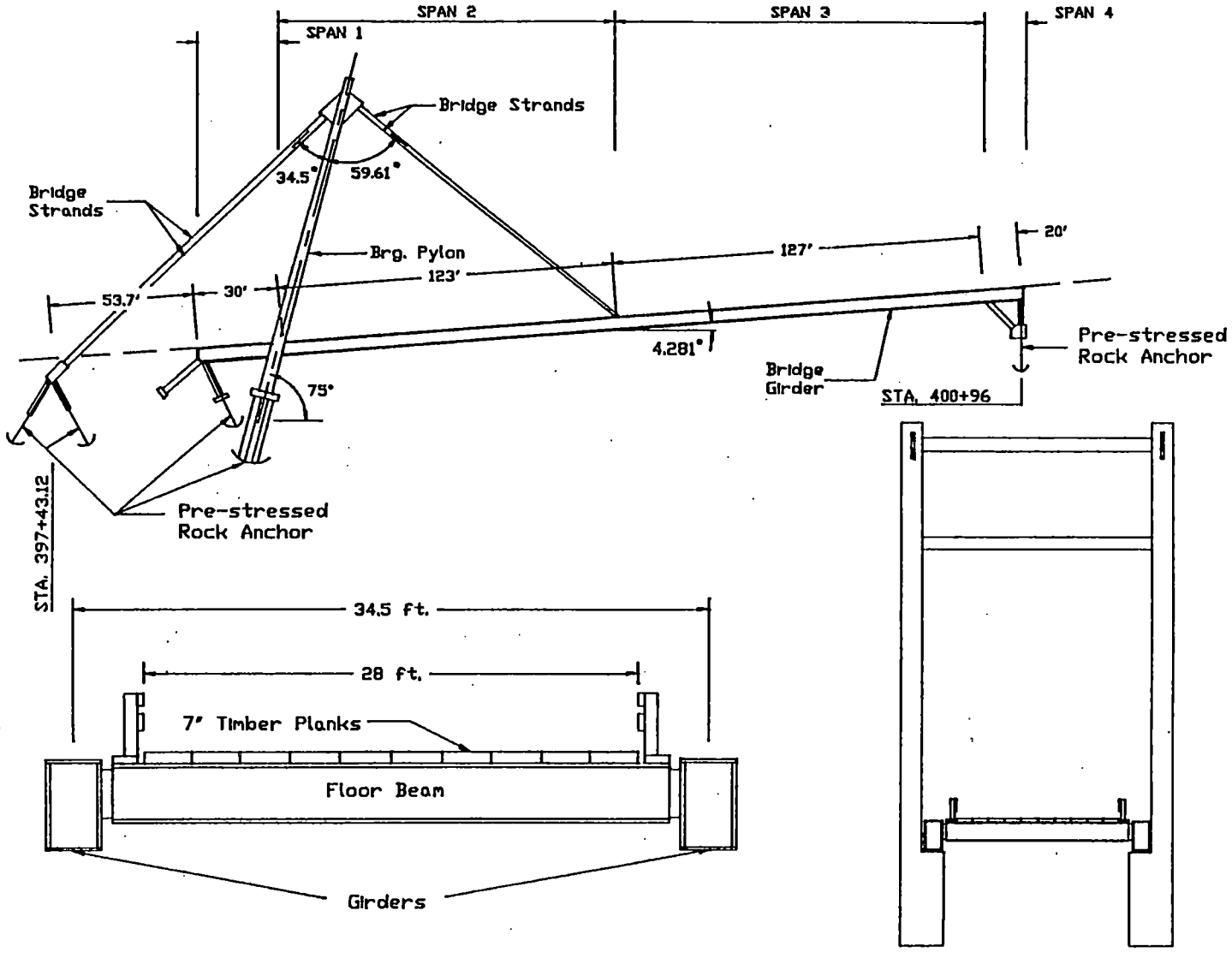

Figure 1.1 Moore Creek Bridge Geometry

at approximately 15 degrees to the vertical. The back stays terminate at tripod supports which are mounted down station of the structure and affixed to the hillside by prestressed rock anchors (see Figure 1.1). The structure was originally designed for AASHTO HS15–44 highway loads in 1974. In 1986, the bridge was strengthened to carry loaded ore trucks weighing approximately 160,000 lb. traveling from the Yukon Territory in Canada to Skagway (Hulsey et al.(1990)).

1.3 Types of Static Behavior Investigated

This research is a continuation of several studies employing a static analysis previously conducted on the Captain William Cooper Moore Creek Bridge (Hulsey, Delaney, and Briggs(1990); Hulsey and Delaney(1990); Hulsey et al.(1990)). Because of the unusually large ore truck (B–Train) loadings, and fracture critical design, it was necessary to gain information concerning boundary conditions and the possible over stressing of critical members. Each phase of this study has given further insight into the true behavior of this complex structure.

Investigation into the behavior of this bridge began with instrumentation and experimental field testing under actual bridge loadings. The 160,000 lb. B–Trains were placed at three predetermined locations longitudinally along the bridge. These positions resulted in loads that were both symmetrically and eccentrically placed with respect to the bridge center line. Girder strains and deflections were monitored during the testing period. Strains were also recorded for the tower (pylon) base and an upstation column support(Hulsey, Delaney, and Briggs(1990); Hulsey et al.(1990)). To supplement the experimental investigation and gain a better understanding of the boundary conditions and load distribution, a two–dimensional linear elastic finite element analysis was then performed and the results were compared with experimental findings (Hulsey and Delaney(1990)). The following section presents selected details of the 2–D investigation only with the intent to give the reader an understanding of the analysis performed. For verification and justification of information provided the reader is referred to Hulsey and Delaney (1990).

1.3.1 Two–Dimensional Behavior

A two–dimensional linear elastic analysis (i.e. neglecting geometric nonlinearities) of the Moore Creek Bridge was performed following an experimental study . Principles of statics were used to calculate the distribution of loads to the girders. B–Train axle loads determined by weighing each truck at a nearby weigh station were distributed first to the appropriate floor beams and then to each girder. The girder loads were then used as nodal point loads in the analysis. Results were compared to experimental results with good correlation. Findings and conclusions provided in this section have been taken from the report by Hulsey and Delaney (1990).

A parametric study conducted while developing the 2–D model detected that the bearing configuration at the girder–pylon interface had a significant affect on girder strains. The bearing included a one inch thick neoprene elastomeric bearing pad and a curved steel plate arrangement. Construction details indicated only the neoprene pad was supporting the girder but the comparison of analytical results with experimental data showed both elements were contributing to the transfer of load. Specific findings surrounding the comparison of computed vs. experimental results along with the parametric study are:

1. The behavior is significantly influenced by the support conditions. For example, supports with prestressed rock anchors behaved as fixed supports and those without behaved as pinned supports.
2. The bridge behavior is significantly influenced by the interaction between the curved steel plate and the elastomeric bearing pad at the girder pylon interface. The results are influenced by the deformation of the neoprene pad.
3. The bridge behavior can be accurately approximated with a 2–D model for symmetric loads.
4. Accurate prediction of the behavior produced by the lane loads (asymmetric loads) will require a 3–D model.

Statements 1 and 2 above were based upon a parametric study conducted while developing a model which best approximated results of the experimental investigation. Statements 3 and 4 above were based upon the comparison made once the final analytical model had been developed. A comparison between experimental and 2–D analytical results showed that excellent correlation could be achieved for symmetrical loading conditions (B–Train on bridge center line). However, when loads for eccentrically placed B–Trains (in right or left lane) were distributed as described above, the computed strains and deflections of the girder nearest the load were considerably larger than those measured in the field. Also, the computed strains and deflections of the girder farthest from the load were considerably smaller than those measured. This implied that either the two–dimensional model did not account for the interaction of opposite sides of the bridge under eccentric loading conditions, or the method of statics used to distribute the loads to each girder was not valid. Plate action of the timber plank deck was not accounted for in the load distribution to the box girders. It was anticipated that if plate action of the deck was accounted for it would tend to spread out the load. More load would be transferred to the girder on the opposite side of the bridge from the load and even out girder deflections. The effect of this load distribution will require further studies. Shear type connectors were used to attach the floor beams to the box girders and will also effect the transfer of forces to each girder. Use of statics assumed the floor beams behaved as simply supported members. The shear type connectors used will restrain floor beam end rotation to some degree but do not completely restrain rotation. Load transfer via these connections will lie somewhere between fixed end forces and simply supported reactions. In view of these findings it was decided a three–dimensional analysis should be conducted.

1.3.2 Three–Dimensional Behavior

Results of a 2–D analysis on the Moore Creek Bridge indicated the 3–D response to eccentrically applied loads should be investigated. When statics principals were used to distribute asymmetric loads, assumptions of two–dimensional models could not account

for redistribution of loads resulting from the torsional rigidity of the bridge deck system. Modeling one side or the other alone did not account for interaction between the two when loads were not shared equally. It was felt that modeling the structure three–dimensionally might improve analytical results for eccentric loadings. Results would change less for symmetric loadings. Under symmetric loads, two–dimensional and three–dimensional results should be equal within modeling tolerances. Therefore the three–dimensional model was constructed by connecting two–dimensional model geometry of each side with floor beams, cross bracings, etc. In order to make a consistent comparison between models, boundary conditions, girder/pylon bearing configuration, and other details of the final two–dimensional model remained unchanged in the three–dimensional model used in this latest study. Model details, analysis and comparison results, and study findings are presented in following sections of this report.

Discrepancies between two–dimensional analytical results and experimental data were small. It was thought that some of this difference might resulted from cable geometric nonlinearities. Thus an element for modeling cable behavior was developed and incorporated into a three–dimensional finite element program. This provided for the investigation to evaluate the contribution of cable geometric nonlinear influence in the Moore Creek Bridge.

1.3.3 Geometric Nonlinearities of Cables

Geometric nonlinearities of inclined cables are associated with large displacements (drape) of a cable under its own weight or externally applied distributed loads. The degree of drape varies nonlinearly with cable tension. If cable tension is such that no drape is present and the material has not been stressed beyond its proportional limit, when additional load is applied the cable behaves as an axial truss member experiencing stress and strain along its major axis only. When a cable under equilibrium conditions is not taut but in some initial deformed position, changes in the state of stress due to changes in load is no longer linear because second order strain components are no longer insignificant.

A cable–stayed bridge is at an initial equilibrium state of stress with cable post–tensioning forces before live loads are applied. Assuming the cables, prior to live load application, are not stressed beyond their proportional limit, and knowing their post–tensioning force and unit weight, the effective cable stiffness can be derived by determination of the deformed position. Live loads are distributed throughout the structure, according to the relative stiffness of the members, to achieve a new state of equilibrium. In response to a change in stress, cable deformed positions may move changing the cable effective stiffness. Final cable effective stiffness is consistent with the cable deformed position which corresponds to the new equilibrium state of stress of the bridge.

Understanding this behavior formed the basis by which the element for modeling cables of the Moore Creek Bridge was developed. A FORTRAN program was written which computes cable effective stiffness knowing a cable's tension, unit weight, and initial end positions. With cable stiffness known for a given tension, the bridge was analyzed and cable forces examined. If cable forces changed, a new equilibrium deformed position was established and corresponding effective stiffness determined. The structure was reanalyzed and computed cable forces were checked for each iteration until cable tensions converged. Formulation of element stiffness relations, development of a cable modeling routine, and integration with a three–dimensional finite element program are presented in Chapters 3, 4, and 5 respectively.

It is important to note that only geometric nonlinearities associated with the cables were investigated. A cable–stayed bridge can also experience large displacements in the girders and tower configuration as well. Analysis incorporating geometry changes or moving coordinates of beam elements were not included in this study. If these effects were included a new stiffness matrix would be required for the entire structure through each iteration cycle. When final equilibrium was achieved the final deformed location of each point would be known.

2. HISTORY OF MODELING CABLES

The analysis of structural systems composed of cables has been of interest for years. Nonlinear strain-displacement relationships produced by large displacements exist in cable members and these effects introduce analytical complexities. A wide range of methods have been suggested in the literature for approximating the effects of geometric nonlinear behavior in a structure containing cables. These methods vary with simplifying assumptions and solution techniques.

Cable nonlinearities have been approximated by linear analysis techniques by using an effective modulus in the analysis of cable–stayed bridges (Lazar(1972); Maceri and Como(1985)). Fictitious or imaginary loads which correct effects of cable tension forces on the structure for the cable nonlinear behavior have been used to analyze cable–stayed bridges and transmission towers (Tang(1971); Fang et al.(1979); Rosenthal and Skop(1980)).

Fang et al.(1979) analyzed guyed transmission towers using catenary expressions to develop cable stiffness relationships. The stiffness expressions related horizontal and vertical tension components, at a cable's end, to changes in end point position. These tension forces were applied to the tower at guy attachment points. Cable nonlinearities were accounted for in an iterative process by adjusting cable stiffness and computing new tension forces resulting from end translations. The procedure was developed for designing guyed structures. The development was restricted to the assumption that initial tension was known and that cable loading was restricted to: a) end tension; and b) a uniform distributed load per unit length.

Various techniques of the stiffness method of structural analysis have been used by others to develop general and versatile techniques for cable–stayed systems. Several authors have idealized the cables of a structure with straight two–node axial elements (Baron and Venkatesan(1971); Argyris and Scharpf(1972)). Reported studies show these type of elements were used to analyze cable–stayed structures (Cheung(1984); Crawford and

Loris(1984)). Another development similar to the one used in this report applied energy principals in a general formulation to analyze geometric nonlinearities (Henghold and Russel(1976)). The development, based on the principal of virtual work, provided for a family of nonlinear elements to determine equilibrium static deflections and natural frequencies of cable structures.

A report which had a large impact on the analysis of cable structures (Peyrot and Goulois(1979)) used a numerical procedure based on exact relations (catenary). The presentation provides a single efficient cable element subprogram which computes element end forces, its deformed position and stiffness. Displacements are restricted to a single plane in the direction of the resultant of external applied uniform distributed forces and cable weight. Use of this element for the research reported herein was examined, but as presented, the variables required for input differed from the needs of this research. The subprogram is based on the assumption that the cable unstressed length is known and this project relies on knowing cable tension at its lowest end. Other differences exist between Peyrot's element and the one developed in this report. Some of the differences are presented below. Peyrot's catenary element only allows loads to be uniformly distributed along its length or applied at end nodes. Intermediate concentrated loads require additional elements with end nodes at points of load application. The three–node element presented herein allows the same loads as well as concentrated loads at its middle node. Another difference is the three–node element reported herein is capable of modeling linear axial truss members taking compression as well as tension. The formulation presented in section 3.2 of this report can also be modified and the three–node element would be capable of displacements in all directions allowing for general loading conditions.

An element which provided for the particular needs of this research was not available in the literature. In order to investigate geometric nonlinear influence of cables in the Moore Creek Bridge, an element was desired which accounted for elastic, initial stress, and large–deflection influences on cable stiffness. These stiffness components also had to

be obtainable from available information about the bridge. (i.e.; cable post–tension at lowest end, cable weight, and end point locations.) Methods reported above were either not amenable to a finite element analysis, or formulated in such a way that unavailable variables (i.e.; cable length and initial deformed position) were required. Therefore, decision was made to formulate an element which related a member's state of stress to its nodal displacements, relative to an initial undeformed position assumed to lie along a straight line between its end points. Thus, the initial coordinates of an element's nodes could be easily obtained from the cable end point coordinates. The formulation also allowed for using the same element for linear as well as nonlinear analysis.

3. ELEMENT FOR MODELING CABLE–STAYS

3.1 Development Theory

Cables of a cable–stayed bridge are normally inclined and under some post–tension. For a given cable unit weight, tension force, and end coordinates, an equilibrium deformed position of the cable exists. The effective stiffness of the cable corresponds to the deformed state. When live loads are applied to the bridge, forces are redistributed throughout the structure in accordance with the stiffness of each member. If tension in the cable members changes so will their deformed configuration. This results in an adjustment to their effective stiffness. Forces in the structure redistribute until a state of equilibrium is reached. Therefore, an element was developed which for a given lowest end tension force, unit weight, and end coordinates will model the effective stiffness of a cable. An incremental–iteration type solution was incorporated and proceeded as follows:

1. Initial cable stiffness based upon post–tension force was determined;
2. Bridge was next analyzed for a given live load condition;
3. Computed force in cable elements were added to the cable post–tensioning forces;
4. Cable stiffnesses were recomputed and the structure was reanalyzed;
5. New computed cable forces were compared with that from the previous iteration;
6. If not within the convergence criteria ($\leq 0.5\%$), steps 3 – 5 were repeated; and
7. The solution was continued until the difference between new computed cable forces and that of previous iteration was sufficiently small.

A three–node axial element was selected for modeling cable behavior. It was shown by other researchers (Irvine(1975); Krishna(1978)) that the geometry of a freely suspended cable can be approximated by a parabola. A comparison with the exact (catenary) shape shows that this approximation is sufficiently accurate for use with cables with reasonable central sag to span ratios (Krishna(1978)). The shape function consistent with the displacement field of a three–node axial element is a second degree polynomial. Therefore, the element displacement field contains the parabolic shape (Figure 3.1).

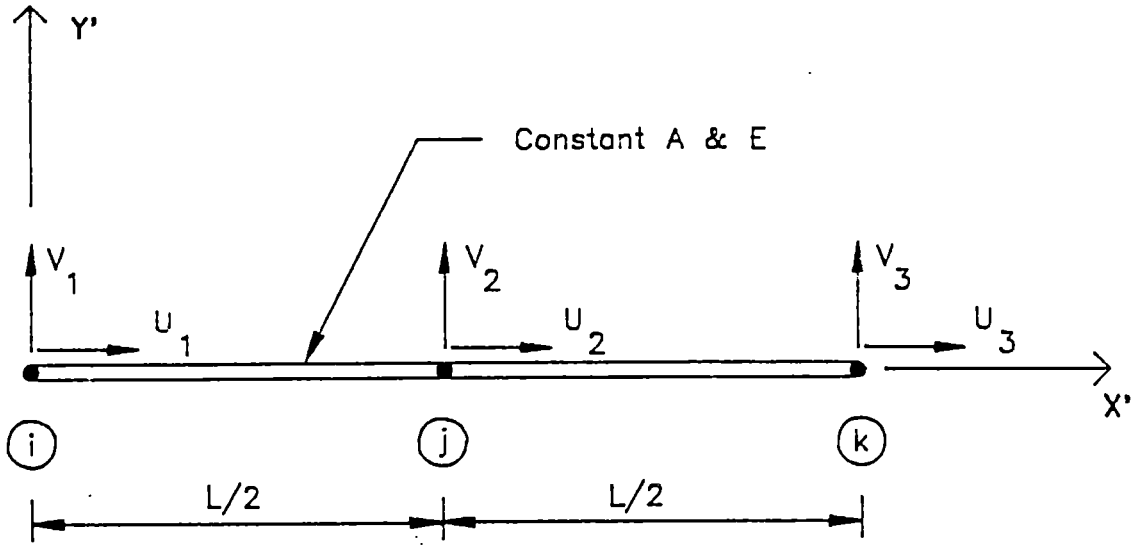

a) Local Degrees of Freedom

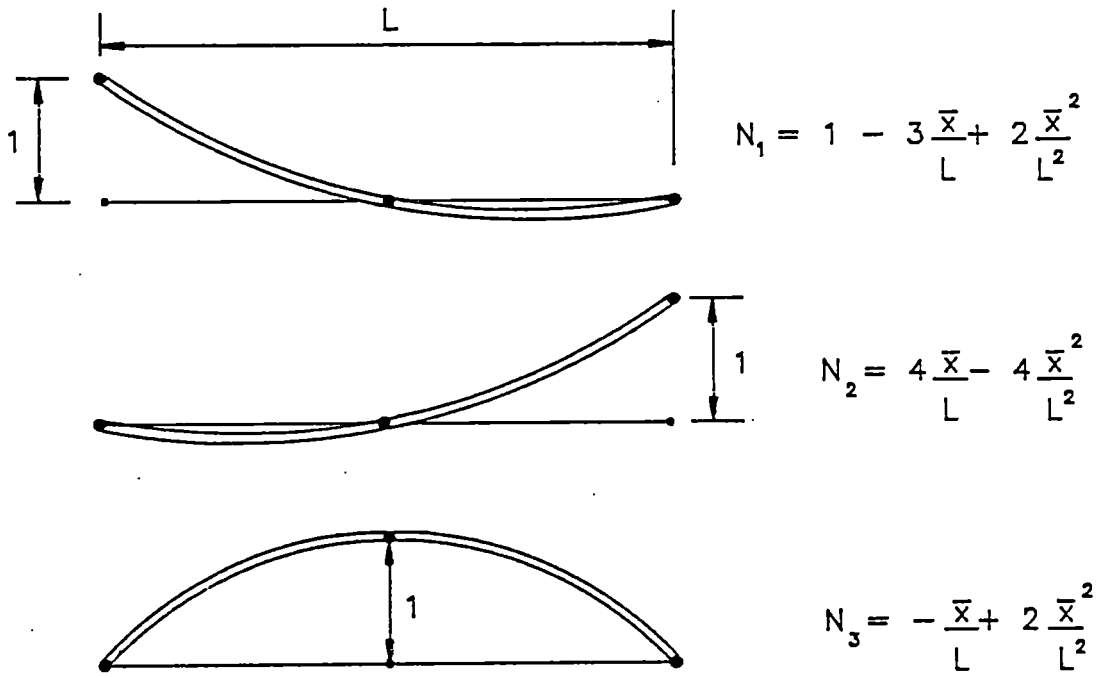

b) Shape Functions

Figure 3.1 Cable Element. a) Local Degrees of Freedom; b) Shape Functions

Only axial strains and second order strains associated with large–deflections in the local Y' direction (V_i's) were considered. Displacements were restricted to a vertical plane containing the cable end points. Thus the element has two local degrees–of–freedom per node, and functions describing local displacements along the element in both orthogonal directions, $U(x)$ and $V(x)$, were based upon the parabolic shape functions. Figure 3.1a shows the undeformed element and its local degrees–of–freedom, and Figure 3.1b describes the parabolic shape functions used.

Derivation of element stiffness was based on a displacement formulation approach using variational principals (Zienkiewicz(1981)). Parts of the formulation are detailed in Section 3.2 and are presented only to give the reader a conceptual understanding of the theory. For a more complete description the reader is referred to (Zienkiewicz(1981)).

3.1.1 Assumptions and Limitations

This element was developed specifically for modeling cables of the Captain William Cooper Moore Creek Bridge. Only geometric nonlinearities associated with cables were accounted for. Assumptions and limitations of the cable element are:

1. The material is elastic (Hooke's law applies);
2. The material is homogeneous and isotropic;
3. Element section properties are constant throughout its length;
4. Only axial strains and second order strains associated with large–deflections in the local Y' direction are considered;
5. Displacements are restricted to a single vertical plane;
6. Cable end displacements between iterations are negligible;
7. Tension at lowest end of the cable, unit weight, and end point coordinates are known or can be determined, and must be a realistic combination;
8. External applied cable loads must be vertical concentrated nodal point loads or uniform distributed loads added to cable weight;

9. The element is limited to axial tension forces for nonlinear analysis, and axial tension or compression for linear analysis;
10. Only static loads are accounted for.

Some of the above items warrant further discussion of their applicability and validity.

Item #4. The assumption is justifiable although other second order components of strains exist. Without considering nonlinearities of cable material or composition, only second order axial strains exist and are here considered negligible.

Item #6. Only cable geometric nonlinearities were investigated. Thus, if a node was not affixed to a support, final end point positions were not known until equilibrium of the structure is reached. Adjustment for cable end movements would not be valid during intermediate cycles. It would have been necessary to include complete structure geometric nonlinearities by a method of moving coordinates to account for end displacements.

Item #7. The investigation of the effect of these variables was the purpose of developing the element. The accessible point for measuring cable post–tension force in a cable–stayed bridge is primarily its lowest end. This is the location where cable post–tension forces were measured by others for the cables of Moore Creek Bridge. The finite element program (presented in Chapter 4) utilizes exact (catenary) relations for computing end reactive forces. These forces are required to hold the cable in equilibrium with its tension and self–weight. Therefore, equilibrium must be possible under the combination of these variables.

3.2 Element Stiffness Formulation

The approach used is a displacement formulation based on standard variational principals (Zienkiewicz (1981)). A three–node axial element was selected to model cable–stays the for reasons previously stated. Element strains include axial and large–deflection components. The formulation is in reference to a local, X' and Y', coordinate system (see

Figure 3.1). Stiffness and displacements require transformation to the proper global coordinate system.

Allowing the element to displacement along its length in accordance with a second order polynomial, the displacement field $\mathbf{U}$ of the element is given by, (bold variables designate matrices; e.g. $\mathbf{U} = \{U\}$)

$$\mathbf{U} = \mathbf{N}\,\mathbf{U_N} \tag{3.1}$$

or expanded,

$$\mathbf{U} = \begin{Bmatrix} U(\bar{x}) \\ V(\bar{x}) \end{Bmatrix} = \begin{bmatrix} N_1 & 0 & N_2 & 0 & N_3 & 0 \\ 0 & N_1 & 0 & N_2 & 0 & N_3 \end{bmatrix} \begin{Bmatrix} U_1 \\ V_1 \\ U_2 \\ V_2 \\ U_3 \\ V_3 \end{Bmatrix} \tag{3.1a}$$

Where $\mathbf{U_N}$ is a $6x1$ vector of the nodal point displacements and $\mathbf{N}$ is a $2x6$ matrix which contains the interpolation (shape) functions (see Figure 3.1b). The element axial strain ϵ_{xx} based on Large–Deflection Strain–Displacement relations is given as (Przemieniecki(1968)),

$$\epsilon_{xx} = \frac{\partial}{\partial \bar{x}} U(\bar{x}) + \frac{1}{2}\left(\frac{\partial}{\partial \bar{x}} V(\bar{x})\right)^2 \tag{3.2}$$

where second order axial strains were considered negligible, and $U(\bar{x})$ and $V(\bar{x})$ are the displacement functions in the local X' and Y' directions respectively. The element strain ϵ is considered to have two components; elastic $\epsilon_{\mathbf{E}}$ and large–deflection $\epsilon_{\mathbf{L}}$, which are defined by,

$$\epsilon = \epsilon_{xx} = \epsilon_{\mathbf{E}} + \epsilon_{\mathbf{L}} \tag{3.3}$$

$$\epsilon_{\mathbf{E}} = \frac{\partial}{\partial \bar{x}} U(\bar{x}) = \mathbf{B_E}\,\mathbf{U_N} \tag{3.4}$$

where,

$$\mathbf{B_E} = [\, \tfrac{\partial}{\partial \bar{x}} N_1 \quad 0 \quad \tfrac{\partial}{\partial \bar{x}} N_2 \quad 0 \quad \tfrac{\partial}{\partial \bar{x}} N_3 \quad 0 \,] \tag{3.4a}$$

$$\epsilon_{\mathbf{L}} = \frac{1}{2}\left(\frac{\partial}{\partial \bar{x}} V(\bar{x})\right)^2 = \frac{1}{2}\mathbf{B}(\mathbf{U_N})_{\mathbf{L}}\, \mathbf{U_N} \tag{3.5}$$

where,

$$\mathbf{B}(\mathbf{U_N})_{\mathbf{L}} = \mathbf{B_L} = [\, 0 \quad \tfrac{\partial}{\partial \bar{x}} N_1 \tfrac{\partial}{\partial \bar{x}} V(\bar{x}) \quad 0 \quad \tfrac{\partial}{\partial \bar{x}} N_2 \tfrac{\partial}{\partial \bar{x}} V(\bar{x}) \quad 0 \quad \tfrac{\partial}{\partial \bar{x}} N_3 \tfrac{\partial}{\partial \bar{x}} V(\bar{x}) \,] \tag{3.5a}$$

Therefore,

$$\epsilon = (\mathbf{B_E} + \frac{1}{2}\mathbf{B_L})\, \mathbf{U_N} \tag{3.6}$$

The sum of external and internal generalized forces $\mathbf{Q}(\mathbf{U_N})$ of the element is expressed as,

$$\mathbf{Q}(\mathbf{U_N}) = \int_V \mathbf{B_T}^{\mathbf{T}}\, \sigma\, dv - \mathbf{f} = 0 \tag{3.7}$$

where $\mathbf{f}$ = external applied forces, σ = element stress, and $\mathbf{B_T}$ is defined by,

$$\mathbf{d}\epsilon = \mathbf{B_T}\, \mathbf{dU_N} \tag{3.8}$$

and it can be shown that,

$$\mathbf{B_T} = \mathbf{B_E} + \mathbf{B_L} \tag{3.9}$$

Taking the proper variation of Eqn. 3.7 above gives,

$$\mathbf{dQ}(\mathbf{U_N}) = \int_V \mathbf{dB_T}^{\mathbf{T}}\, \sigma\, dv + \int_V \mathbf{B_T}^{\mathbf{T}}\, \mathbf{d}\sigma\, dv = 0 \tag{3.10}$$

Considering only linear elastic materials, stress is written as,

$$\sigma = \mathbf{D}(\epsilon - \epsilon_o) + \sigma_o \tag{3.11}$$

where $\mathbf{D}$ = contains constitutive properties, ϵ_o = initial strain, and σ_o = initial stress. Using Eqns. 3.9 and 3.11 the following is obtained,

$$\mathbf{dB_T} = \mathbf{dB_L} \tag{3.12}$$

$$\mathbf{d}\sigma = \mathbf{D}\,\mathbf{d}\epsilon \tag{3.13}$$

For axial strains $\mathbf{D} = E$, Young's Modulus of Elasticity. Substituting Eqn. 3.8 into Eqn. 3.13 and using the result in Eqn. 3.10 gives,

$$\mathbf{dQ(U_N)} = \int_V \mathbf{dB_L}^{\mathbf{T}}\,\sigma\,dv + E\int_V \mathbf{B_T}^{\mathbf{T}}\,\mathbf{B_T}\,\mathbf{dU_N}\,dv = \mathbf{K_T}\,\mathbf{dU_N} \tag{3.14}$$

The matrix $\mathbf{K_T}$ is called the Tangential Stiffness Matrix and includes elastic, $\mathbf{K_E}$, large–deformation, $\mathbf{K_L}$, and initial stress, $\mathbf{K}_\sigma$, stiffness components.

Inserting Eqn. 3.9 into Eqn. 3.14 and separating the second integral into elastic only terms and terms containing large–deformation expressions gives relations for elastic stiffness, $\mathbf{K_E}$, and large–deformation stiffness, $\mathbf{K_L}$, stiffness components.

$$\mathbf{K_E} = EA\int_0^L \mathbf{B_E}^{\mathbf{T}}\,\mathbf{B_E}\,d\bar{x} \tag{3.15}$$

$$\mathbf{K_L} = EA\int_0^L \left(\mathbf{B_E}^{\mathbf{T}}\,\mathbf{B_L} + \mathbf{B_L}^{\mathbf{T}}\,\mathbf{B_E} + \mathbf{B_L}^{\mathbf{T}}\,\mathbf{B_L}\right)d\bar{x} \tag{3.16}$$

In which A = cross–sectional area; and L = elements' undeformed length. Initial stress component of stiffness, $\mathbf{K}_\sigma$, comes from the first integral of Eqn. 3.14 and takes the form,

$$\mathbf{K}_\sigma = A \int_0^L \mathbf{G}^\mathbf{T}\,\mathbf{M}\,\mathbf{G}\,d\bar{x} \tag{3.17}$$

where,

$$\mathbf{G} = [\,0 \quad \tfrac{\partial}{\partial \bar{x}} N_1 \quad 0 \quad \tfrac{\partial}{\partial \bar{x}} N_2 \quad 0 \quad \tfrac{\partial}{\partial \bar{x}} N_3\,] \tag{3.17a}$$

$$\mathbf{M} = [\sigma_i N_1 + \sigma_j N_2 + \sigma_k N_3] \tag{3.17b}$$

Thus, M was a $1x1$ matrix which contains the axial stress function also allowed to vary along the element in accordance with the shape functions. From Eqns. 3.14, 3.15, 3.16, and 3.17, $\mathbf{K_T}$ becomes,

$$\mathbf{K_T} = (\mathbf{K_E} + \mathbf{K_L} + \mathbf{K}_\sigma) \tag{3.18}$$

Thus, the relation between change in forces to change in nodal position is given by,

$$\mathbf{dQ} = \mathbf{K_T}\,\mathbf{dU_N} \tag{3.19}$$

or,

$$\mathbf{dU_N} = \mathbf{K_T}^{-1}\,\mathbf{dQ} \tag{3.20}$$

The final set of equations are obtained by assemblage of Eqn. 3.20 for each element within the cable.

An application of the Newton–Raphson method for solving algebraic and transcendental equations was used to solve the assembled set of equations (Cook(1974)). In brief, this process involves successive solutions for $\mathbf{dU_N}$, holding $\mathbf{dQ}$ constant. Nodal displacements in the local Y' direction ($V_i's$) are summed between iterations until computed V_i values become sufficiently small. Element stiffness for each iteration i is computed from

$\sum_{m=1}^{i} (dU_N)_m$ where only local Y' displacements are summed. Once convergence is obtained, total cable tangential stiffness (effective stiffness) is found.

4. SOLUTION TECHNIQUE

A three–dimensional finite element analysis including cable geometric nonlinearities was performed on the Captain William Cooper Moore Creek Bridge. Geometric nonlinear behavior of the cables was accounted for by means of an element developed specifically for this research. An element was needed which would approximate cable geometry and stiffness under a deformed state knowing the cable's tension at its lowest end, unit weight, and end point coordinates. Element stiffness relations were developed using variational principals in a displacement formulation (Zienkiewicz(1981)). When modeling cable geometric nonlinearities, element stiffness is determined using an iterative process. A Newton–Raphson type method was employed here (Cook(1974)). The effective stiffness corresponded to the deformed cable position when cable weight and tension were at equilibrium. Based on the relations presented in Chapter 3, a finite element program was written. The program solves for nodal displacements and iterates until the change in transverse nodal position is less than 0.1%. Final displacements at the cable's equilibrium deformed position include: a) axial displacements computed in the final iteration; and b) the sum of the transverse deflections computed in each previous iteration. The final axial deformations, Ui, and transverse deformations, Vi, give the equilibrated deformed configuration. The cable element tangential stiffness consists of the elastic, initial stress, and large displacement stiffness components. The initial stress component is a function of both U and total V changes in nodal position; the large deflection component is a function only of total V changes in nodal position; and the elastic component remains constant. Final nodal displacements are used to compute total cable effective stiffness. An overview of the procedure is given in the following section and pertinent details of the program and flow diagram of the program are presented later.

4.1 Procedure Concept

1. Based on the assumption that the cable post-tension force was measured at the cable–girder interface (lowest end of the cable), cable weight and cable end coordinates were known, initial local nodal displacements, $\mathbf{dU_{N1}}$, were estimated assuming a parabolic shape between ends (see Figure 4.1). This step was not absolutely necessary. If displacements are initially assumed zero, first iteration results would give an initial set of displacements. However; it was determined by beginning with an initial estimate of the cable's deformed position, fewer iterations were necessary for convergence. This process is further described later.
2. Using exact (catenary) relationships, and based upon initial cable tension, cable weight, and cable end coordinates, global horizontal and vertical reactions necessary to hold the cable in equilibrium with its weight and tension were computed. These reactions were placed in the global force vector $\mathbf{dQ}$ as loads applied to end nodes. Again details are given later.
3. With initial local displacements computed in step 1 above, element stiffness components, $\mathbf{K_E}$,$\mathbf{K_L}$, and $\mathbf{K}_\sigma$, were determined and summed to construct the tangential stiffness matrix $\mathbf{K_T}$ of each element.
4. Tangential stiffness matrices of all elements in the cable were assembled into a total tangential stiffness matrix of each cable.
5. Cable weight was distributed to the nodes by approximating cable length between each node with a straight cord. It was assumed half the cable weight between adjacent nodes acts as a global vertical force at each node. Weight forces were combined with reaction forces to complete the global force vector $\mathbf{dQ}$.
6. The total tangential stiffness matrix was transformed to a global coordinate system. Standard methods of stiffness analysis were used to solve: a) the assembled set of simultaneous equations; and b) compute the change to initial assumed nodal positions.

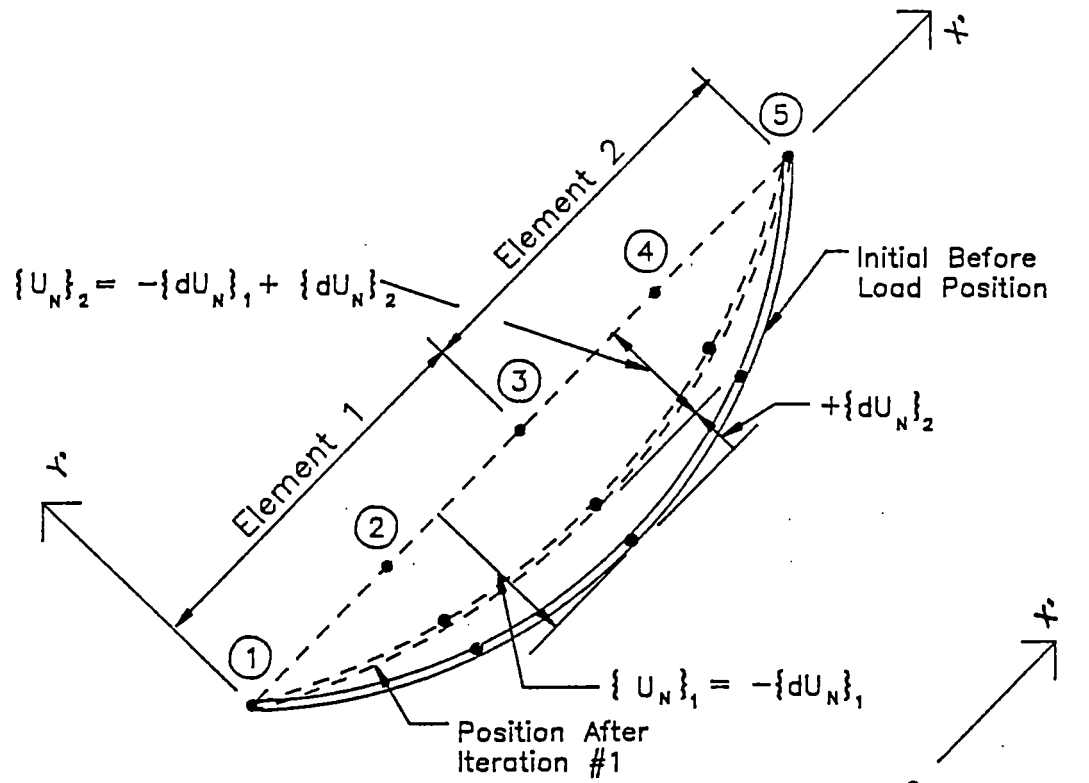

a) First iteration for a 2–element cable.

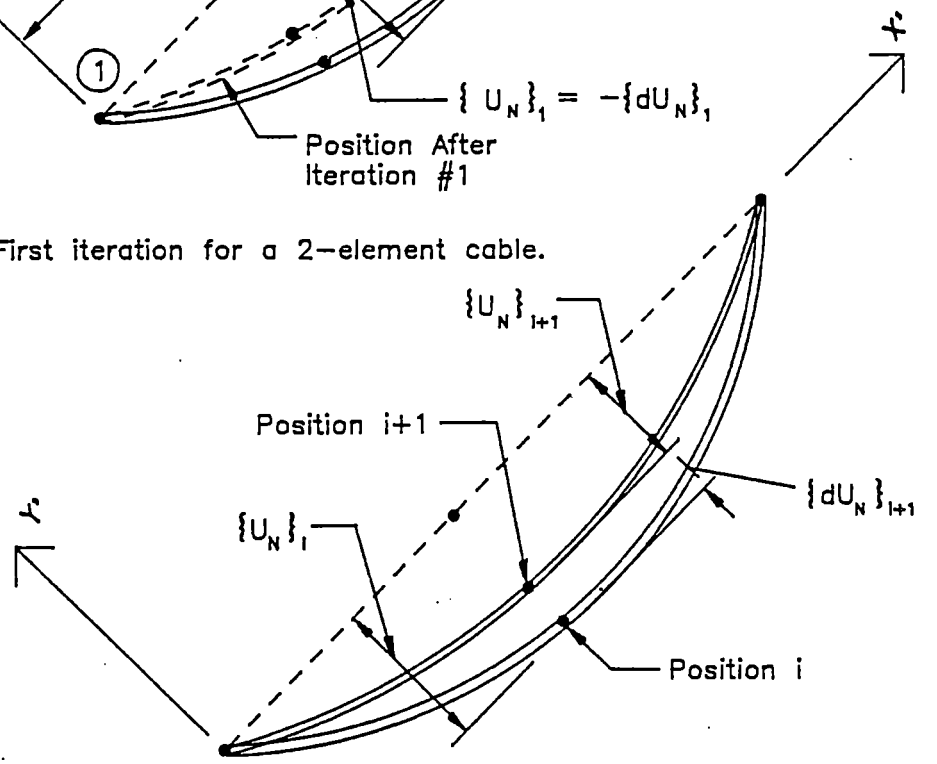

b) Change in cable position after iteration i.

Figure 4.1 Cable Deformed Geometry. a) First Iteration for a 2–Element Cable;

b) Change in Cable Position After Iteration *i*

7. Changes to nodal positions were transformed back to local coordinates $\mathbf{dU_{N2}}$ and transverse components were added to those initially assumed $\mathbf{dU_{N1}}$ (see Figure 4.1a).
8. Since $\mathbf{K_L}$ and $\mathbf{K_\sigma}$ were dependent upon nodal position, their values were updated and a new total tangential stiffness was matrix constructed. Steps 5 – 7 were repeated until the computed change to nodal position was sufficiently small.
9. After convergence was achieved exact (catenary) equations were used to compute true nodal positions, and through trigonometric manipulations exact displacements were compared with final approximate displacements.

The iteration process is summarized as follows (see Figure 4.1.b):

$$\mathbf{dU_{Ni+1}} = \mathbf{K_T}(\mathbf{U_N})_i^{-1}\,\mathbf{dQ} \tag{4.1}$$

$$\mathbf{U_{Ni}} = \sum_{m=1}^{i} \mathbf{dU_{Nm}} \tag{4.2}$$

4.2 Computer Application

A three-dimensional nonlinear finite element program, utilizing only the three–node axial element previously described, was written for determining a cable's stiffness. The program was also used for verifying element stiffness formulation by comparing approximate nodal displacements with exact displacements based upon exact equations (catenary relations). An iteration process was used where changes to nodal position were computed and transverse components summed in each iteration. Effective stiffness of a cable is a function of its deformed geometry and computed based upon final nodal displacements.

The program was written in FORTRAN 77 and can determine the equilibrium position of a cable under its weight, initial tension, and vertical concentrated loads applied at the nodes. Displacements computed were restricted to a vertical plane passing through the cable end points. Input parameters consist of:

1. Number of elements in cable;

2. Number of nodes in cable;
3. Tension in cable;
4. Weight of cable;
5. Beginning node number and coordinates, x, y, and z;
6. End node number and coordinates, x, y, and z.

Node numbering from left to right established direction of local coordinate system and must be sequential. Node numbers increasing from left to right designated local Y' axis positive upward, decreasing from left to right assigned Y' axis positive downward. Element numbering must also proceed sequentially consistent with node numbering (see Figure 4.2).

4.2.1 Program Structure

The program is partitioned into several subroutines. Following is a list of subroutine names and details of their function. A flow diagram of program structure and subroutine interaction will follow.

CABLE – Main line of program. Reserves memory space required and allocates blocks for primary arrays used throughout program. Controls computation sequences through calling numerous subroutines.

CABSET – Called from CABLE, establishes cable orientation from input end point coordinates.

COORDS – Called by CABLE, generates global coordinates and numbering of all interior nodes in accordance with number of elements specified per cable. Initial undeformed position of cable nodes are along a straight line between end points.

This subroutine also determines cable end reactive forces. Assuming one end of the cable is pinned, an algorithm computes horizontal and vertical forces of the free end necessary to hold the cable in equilibrium. These forces are found based on the following catenary relations (Krishna(1978)):

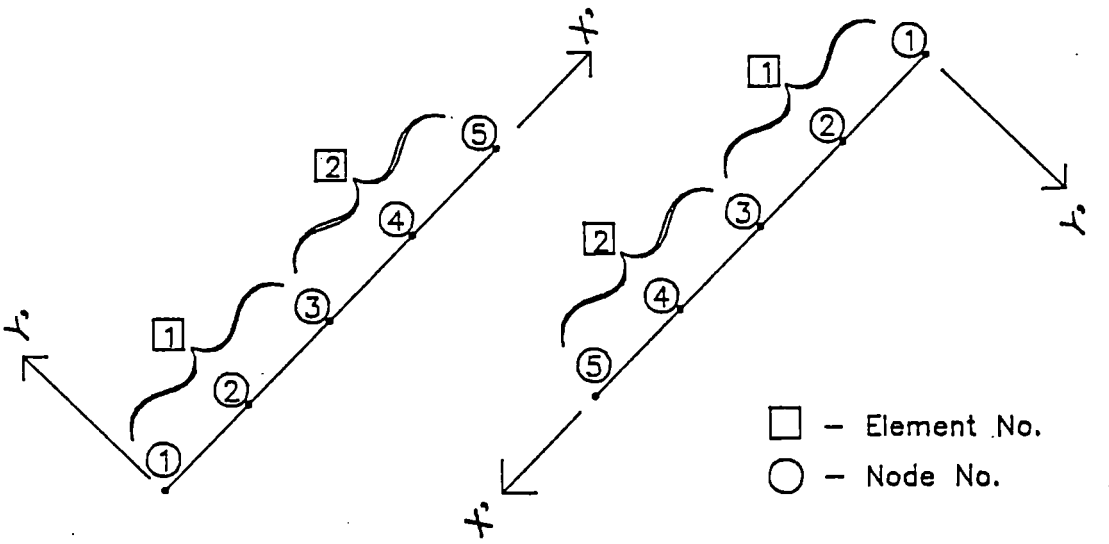

Figure 4.2 Designation of Local Axis

$$z = \frac{H}{q}\left[cosh\alpha - cosh\left(\frac{2\beta x}{X} - \alpha\right)\right] \tag{4.3}$$

$$T' = H\,cosh\alpha \tag{4.4}$$

where,

$$\beta = \frac{qX}{2H} \tag{4.5a}$$

$$\alpha = sinh^{-1}\left[\frac{\beta\frac{|Z|}{X}}{sinh\beta}\right] + \beta \tag{4.5b}$$

In which z = vertical coordinate at horizontal coordinate x; T' = segment tension at upper end; H = horizontal reactive force; q = cable weight per unit length; X = horizontal span of segment; and Z = total vertical rise of segment. The absolute value of Z was used since tension at cables lowest end was assumed to be known. Figure 4.3 shows a cable segment hanging under its own weight at some initial tension. The slope at any point along the segment is obtained from Eqn. 4.3.

$$\frac{dz}{dx} = \frac{H}{q}\left[\frac{-2\beta}{X}\,sinh\left(\frac{2\beta x}{X} - \alpha\right)\right] \tag{4.6}$$

For purposes of obtaining the segments equilibrium deformed position, the left end is assumed restrained against any translations (pinned). Thus, the right end is treated as a free end with horizontal and vertical forces (H and V) of magnitudes such that the segment is in equilibrium with its self–weight and tension. Horizontal forces at the ends must be equal and opposite because it is assumed all external forces act vertical. From a known initial tension (T_{INT}) at cable's lowest end, which acts along a tangent to this end, H can be found by knowing the cable slope at this point. Figure 4.3 shows that the above condition exists when $x = X$. Therefore; from Eqns. 4.5a and 4.6, the slope at a cable's lowest end (ψ), can be found from,

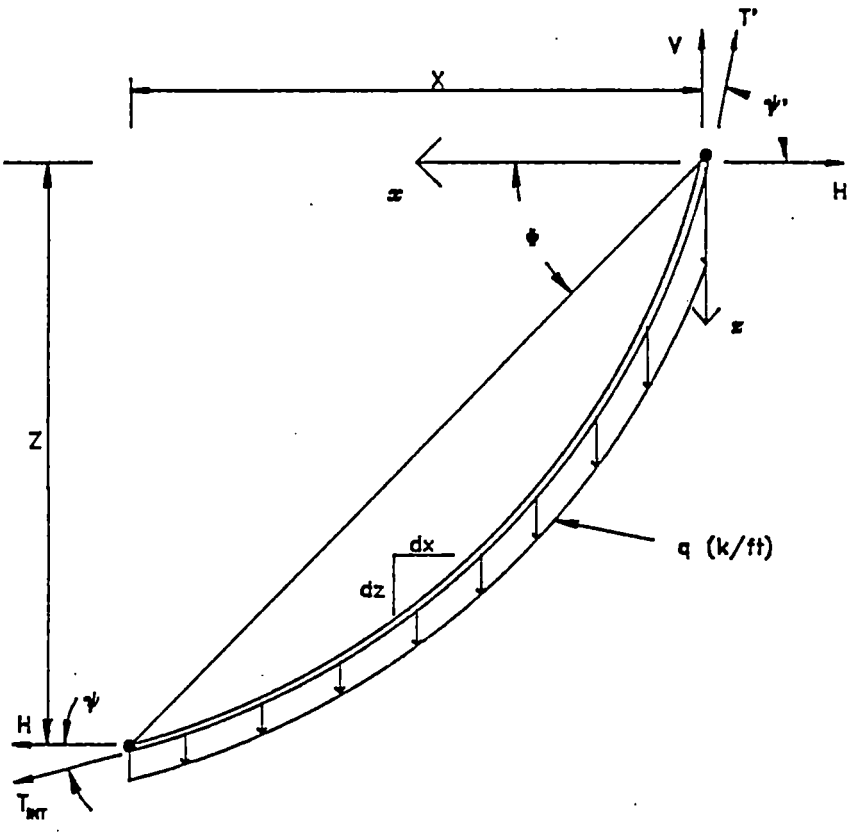

Figure 4.3 Segment of a Catenary

$$\frac{dz}{dx}\Big|_{x=X} = -sinh(2\beta - \alpha) = tan(\psi) \tag{4.7}$$

Thus,

$$H = T_{INT}\, cos(\psi) \tag{4.8}$$

Depending whether the slope (φ) of a straight line between end points is positive or negative, V is obtained from,

$$if; \quad \varphi > 0 \qquad then, \quad V^2 = (T')^2 - H^2 \tag{4.9}$$

$$if; \quad \varphi < 0 \qquad then, \quad V^2 = (T_{INT})^2 - H^2 \tag{4.10}$$

The computer program algorithm approximates an initial value of H by assuming T_{INT} acts along a straight line between end points (at angle φ). The cable end slope is computed and a new value of H determined. Iteration continues until the value of H changes less than 0.01 kips. As stated in the assumptions and limitations of section 3.1.1, cable tension, unit weight, and end point coordinates must be realistically combined. Any length of cable containing weight and suspended from its ends will have some tension force. The tension at a cable's lowest end has a vertical and horizontal component which maintain equilibrium. Catenary relations are derived from the differential equation governing the arc formed by a suspended cable segment in accordance with equilibrium. If a specified combination of weight, tension, and end coordinates do not satisfy these relations, the governing differential equation is violated and the algorithm, therefore, will not converge. For example, if a cable is suspended between two points in a single horizontal plane, and the only force is cable self–weight, the vertical component of the specified tension (T_{INT}) must be equal to or greater than one half the weight of the entire cable or convergence cannot be achieved.

INTDIS – Called from COORDS, computes an initial estimate of nodal point displacements relative to their undeformed position along the cable's cord using a parabolic shape. Referring to Figure 4.4, consider an element of a cable in a vertical plane. The coordinate system in the vertical plane of the cable is denoted by $s - r$. The total cable span and rise are S and R respectively. Points i, j, and k define the element's original undeformed position. Allowing the element to deform under the cable weight, without accounting for elastic deformations, it will displace to position i', j', k' where it remains in equilibrium with the specified tension. Examining node j with coordinates (s_j, r_j), the equation of a line perpendicular to the cable's cord and passing through this point is,

$$r = -\frac{S}{R}s + s_j\left(\frac{R}{S} + \frac{S}{R}\right) \tag{4.11}$$

Assuming a parabolic shape for a cable, with unit weight q and horizontal reaction H, its arc is described by (Krisha(1978)),

$$r = \frac{R}{S}s - \frac{q}{2H}(Ss - s^2) \tag{4.12}$$

The intersection point of lines described by these two equations is found by equating the expressions and solving for s. Then back substitution into either equation completes the coordinates of point j'. Initial transverse displacement V_j can be found from coordinates of points j and j'.

Initial axial displacements U are computed by assuming a cable is undeformed under a constant tension T_{INT}. The axial elongation of a member in tension with a length equal to the length of cable between the pinned end and the node considered (D_{INT}) is given by,

$$U_i = \frac{T_{INT}(D_{INT})_i}{AE} \tag{4.13}$$

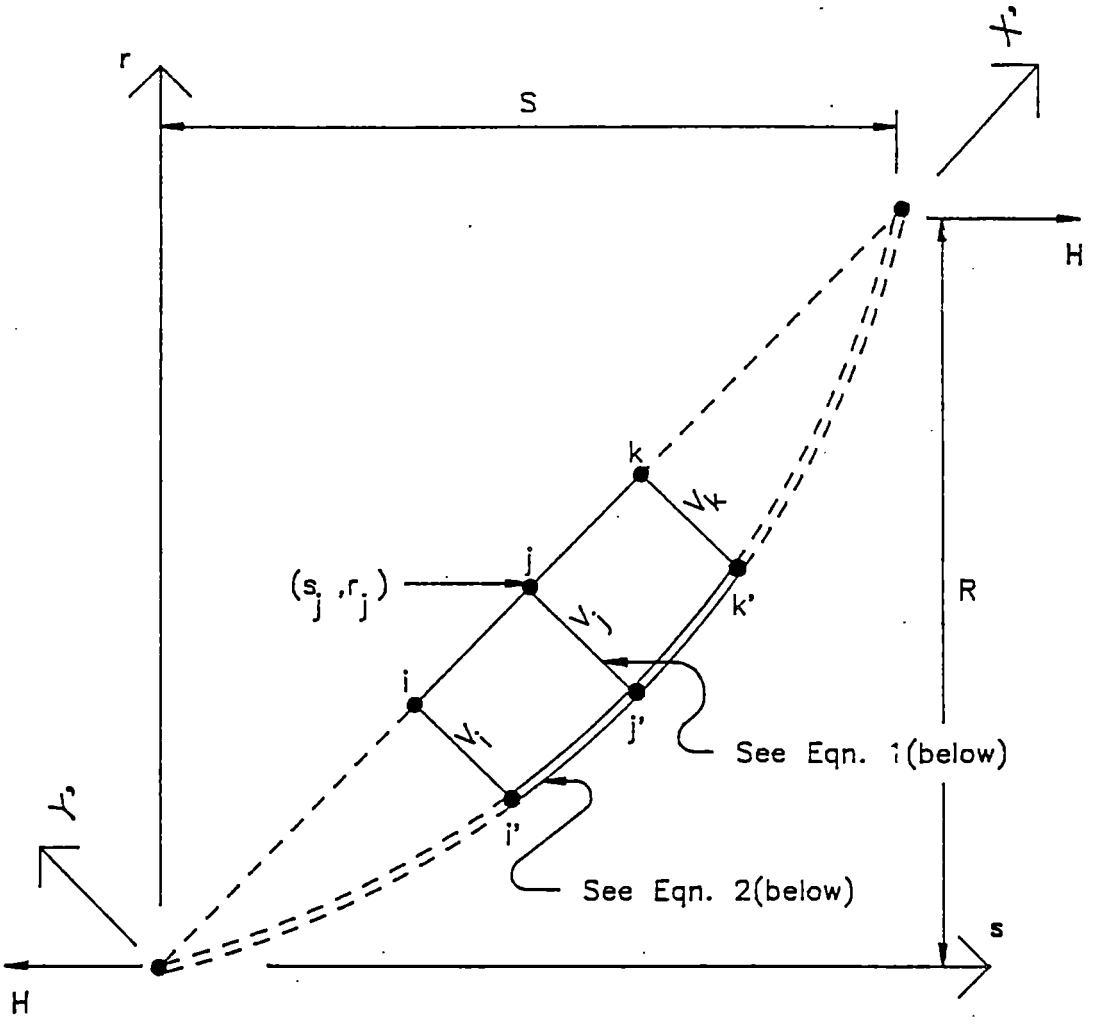

Eqn. 1) $r = -\frac{S}{R}s + s_j\left(\frac{R}{S} + \frac{S}{R}\right)$

Eqn. 2) $r = \frac{R}{S}s - \frac{q}{2H}(Ss - s^2)$

q = cable unit wt.

Figure 4.4 Initial Transverse Nodal Displacements

where T_{INT} = initial tension; D_{INT} = length of cable as described above; A = cable cross sectional area; and E = Young's modulus of elasticity.

ELSETUP – Called by CABLE, generates element numbers and computes directional cosines. Length of each element and its directional cosines with respect to a global coordinate system are established from nodal coordinates. Element incidences and properties are written to an external file for use later.

INTCBEL – Called by CABLE, creates initial cable element stiffness. Calls are made to additional subroutines where initial assumed displacements are used to compute element stiffness components. The elastic stiffness, $\mathbf{K_E}$, initial stress stiffness, $\mathbf{K}_\sigma$, and geometric stiffness, $\mathbf{K_L}$, matrices are combined through a call to an additional subroutine where they are summed to create the element tangential stiffness matrix.

TRANS – Called by INTCBEL, constructs element transformation matrix from directional cosines. Figure 4.5 shows the relation between the six local and nine global degrees–of–freedom.

KELAST – Called by INTCBEL, builds the elastic stiffness matrix $\mathbf{K_E}$. Elements of this matrix remain constant.

KNONLIN – Called by INTCBEL, builds the large deflection matrix $\mathbf{K_L}$. Elements of this matrix are a function of nodal displacements and are updated with each change in node position.

KSIGMA – Called by INTCBEL, builds the initial stress matrix $\mathbf{K}_\sigma$. Prior to calling this subroutine, the stress at each node σ_i, σ_j, and σ_k, each functions of nodal displacement, are computed in INTCBEL. The expressions used for calculating nodal stress were derived from the linear stress–strain relation,

$$\sigma = \mathbf{D}(\epsilon - \epsilon_\mathbf{o}) + \sigma_\mathbf{o} \tag{4.14}$$

The change in stress at the nodal points resulting from a virtual displacement of the nodes is not dependent upon previous states of stress or strain if material behavior is still

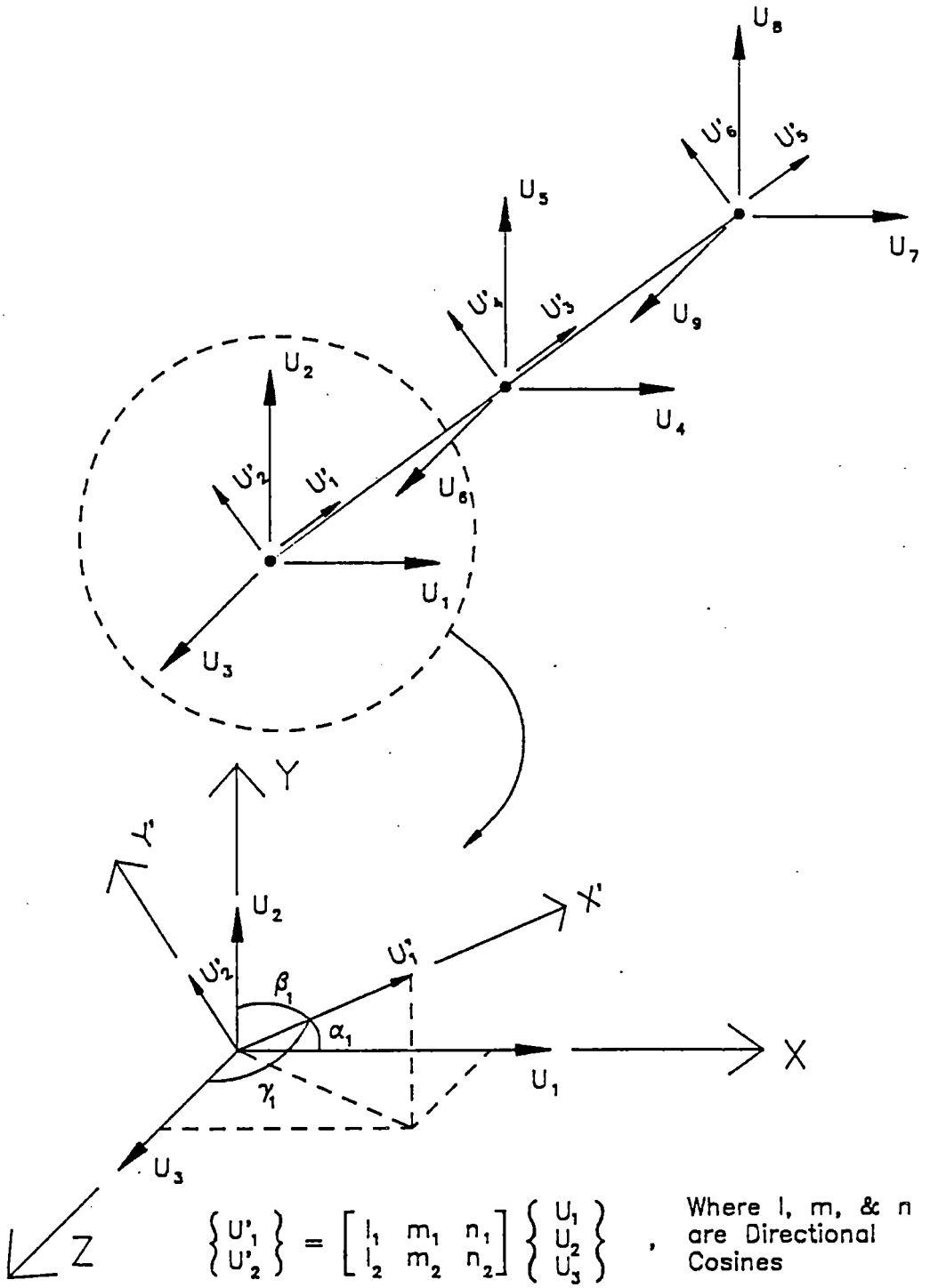

$$\begin{Bmatrix} U'_1 \\ U'_2 \end{Bmatrix} = \begin{bmatrix} l_1 & m_1 & n_1 \\ l_2 & m_2 & n_2 \end{bmatrix} \begin{Bmatrix} U_1 \\ U_2 \\ U_3 \end{Bmatrix}$$

Figure 4.5 Coordinate System Transformation, 2-D Local to 3-D Global

linear and strains are small. The change in stress resulting from a change in strain is given by,

$$\delta\sigma = \mathbf{D}\,\delta\epsilon \tag{4.15}$$

and from Eqn. 3.6,

$$\delta\epsilon = (\mathbf{B_E} + \frac{1}{2}\mathbf{B_L})\,\delta\mathbf{U_N} \tag{4.16}$$

The stress was allowed to vary in accordance with the same second order shape functions as the displacements. Thus,

$$\sigma_i = C_1(-3U_i + 4U_j - U_k) + C_2(9{V_i}^2 + 16{V_j}^2 + {V_k}^2 - 24V_iV_j + 6V_iV_k - 8V_jV_k) \tag{4.17}$$

$$\sigma_j = C_1(U_i - 4U_j + 3U_k) + C_2({V_i}^2 + {V_k}^2 - 2V_iV_k) \tag{4.18}$$

$$\sigma_k = C_1(U_i + 4U_j + 3U_k) + C_2({V_i}^2 + 16{V_j}^2 + 9{V_k}^2 - 8V_iV_j + 6V_iV_k - 24V_jV_k) \tag{4.19}$$

where,

$$C_1 = \frac{E}{L} \tag{4.20a}$$

$$C_2 = \frac{E}{2L^2} \tag{4.20b}$$

Elements of the matrix $\mathbf{K}_\sigma$ are, therefore, a function of nodal displacement and were updated after each iteration.

KTAN – Called by INTCBEL, builds the tangential stiffness matrix $\mathbf{K_T}$. Elastic, large displacement, and initial stress stiffness matrices are algebraically summed. Then using

the local to global transformation matrix, $\mathbf{K_T}$ is transformed to global coordinates through matrix multiplication as follows,

$$\mathbf{K_G} = \mathbf{T^T}\,\mathbf{K_T}\,\mathbf{T} \tag{4.21}$$

where $\mathbf{T}$ is the transformation matrix of directional cosines, and $\mathbf{K_G}$ is the global tangential stiffness matrix.

In order to restrain out of plane bending, an addition transformation or rotation of the coordinate system was required. Removing the degree–of–freedom perpendicular to the cable's plane requires rotating the coordinate system through an angle (θ) about the global Y axis. This aligns the X axis with the cable plane (see Figure 4.6a). Removing the out of plane degree–of–freedom was thus a boundary condition. The program also includes the option of using the element as a truss member. For this purpose, only a single degree-of-freedom existed at each node. Performing an additional coordinate system rotation about the Z_C axis through an angle (φ) allows the transverse degree–of–freedom to also be removed (see Figure 4.6b). Subroutines ROTATE1 and ROTATE2 construct transformation matrices for making these rotations. The appropriate subroutine is called and transformation to the tangential stiffness matrix performed before control is returned to the calling program.

ASEMB – Called by CABLE, assembles element stiffness matrix into a banded total global stiffness matrix for the cable.

CBWTLD – Called by CABLE, calculates loads from cable weight to be applied at each node and adds them in the force vector.

MODIFY – Called by CABLE, modifies the total set of equations for boundary conditions. Out of plane degrees–of–freedom are removed as well as those at the pinned end. Free end reaction forces are add to the force vector.

BANSL – Called by CABLE, solves banded system of equations by Gauss–Elimination process.

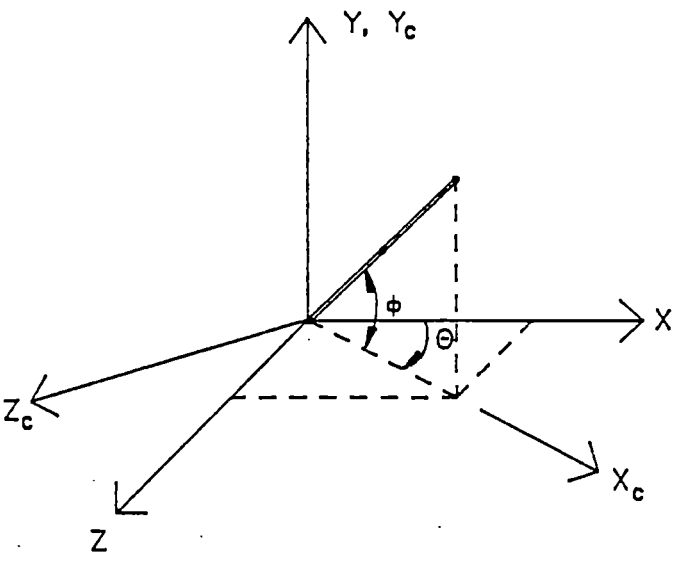

a) Rotation to Cable Plane

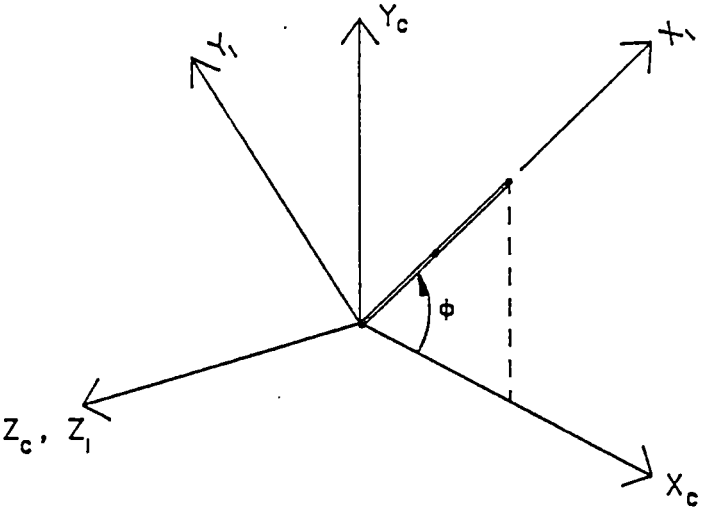

b) Rotation to 3–D Local

Figure 4.6 Rotation of Global Coordinate System. a) Rotation to Cable Plane; b) Rotation to 3-D Local

DISCON – Called by CABLE, converts or transforms computed displacements to the global 3–D coordinate system.

CABEL – Called by CABLE, transforms displacements from global 3–D to local 2–D coordinates and checks for convergence $(V_i / \sum_{j=1}^{n} (V_j)_n \leq 0.1\%)$. If criteria not met, transverse displacements are added to previous total displacements and element stiffness recomputed.

EXACAB – Called by CABLE, calculates exact displacements with catenary equations and compares with final approximate values. Prints out comparison results. It was the purpose of this subroutine to verify solutions with conditions that satisfy exact solutions.

4.2.2 Program Flow Diagram

Figure 4.7 shows the flow chart of PROGRAM CABLE written to establish the equilibrium deformed position of a cable under its self-weight and some initial tension. Figure 4.7a illustrates the manner in which a linear analysis would be performed and Figure 4.7b shows the additional processes performed for a nonlinear analysis.

4.3 Verification Studies

4.3.1 Studies Conducted

A series of studies were conducted to ensure the nonlinear cable element and computer program implementation would accurately predict a cable's behavior. Approximately thirty different cases were examined. Verification studies began by modeling a linear–elastic axial member. First, a one–dimensional study with the member along either horizontal axis, X or Z, using a varying number of elements was studied. For these cases, local and global coordinate systems coincided. Second, the member was inclined at various angles with the horizontal within each orthogonal principal plane examining its linear two–dimensional capabilities. Finally, the member was inclined and rotated about an end through all eight quadrants of the global coordinate system checking the program's ability for three–dimensional analysis. Axial displacements were checked by calculating the axial

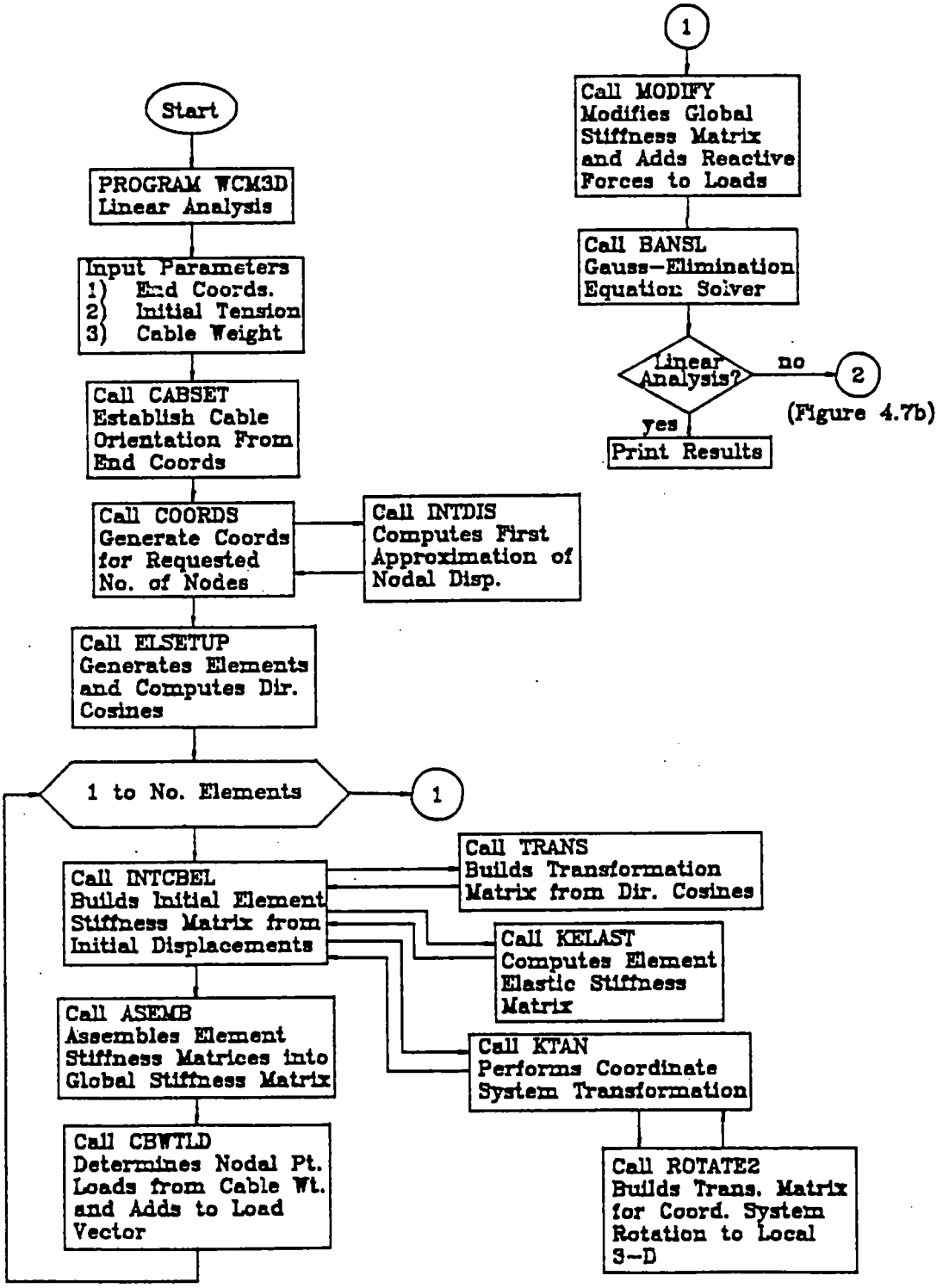

Figure 4.7a CABLE Program Flow Diagram (Linear Analysis)

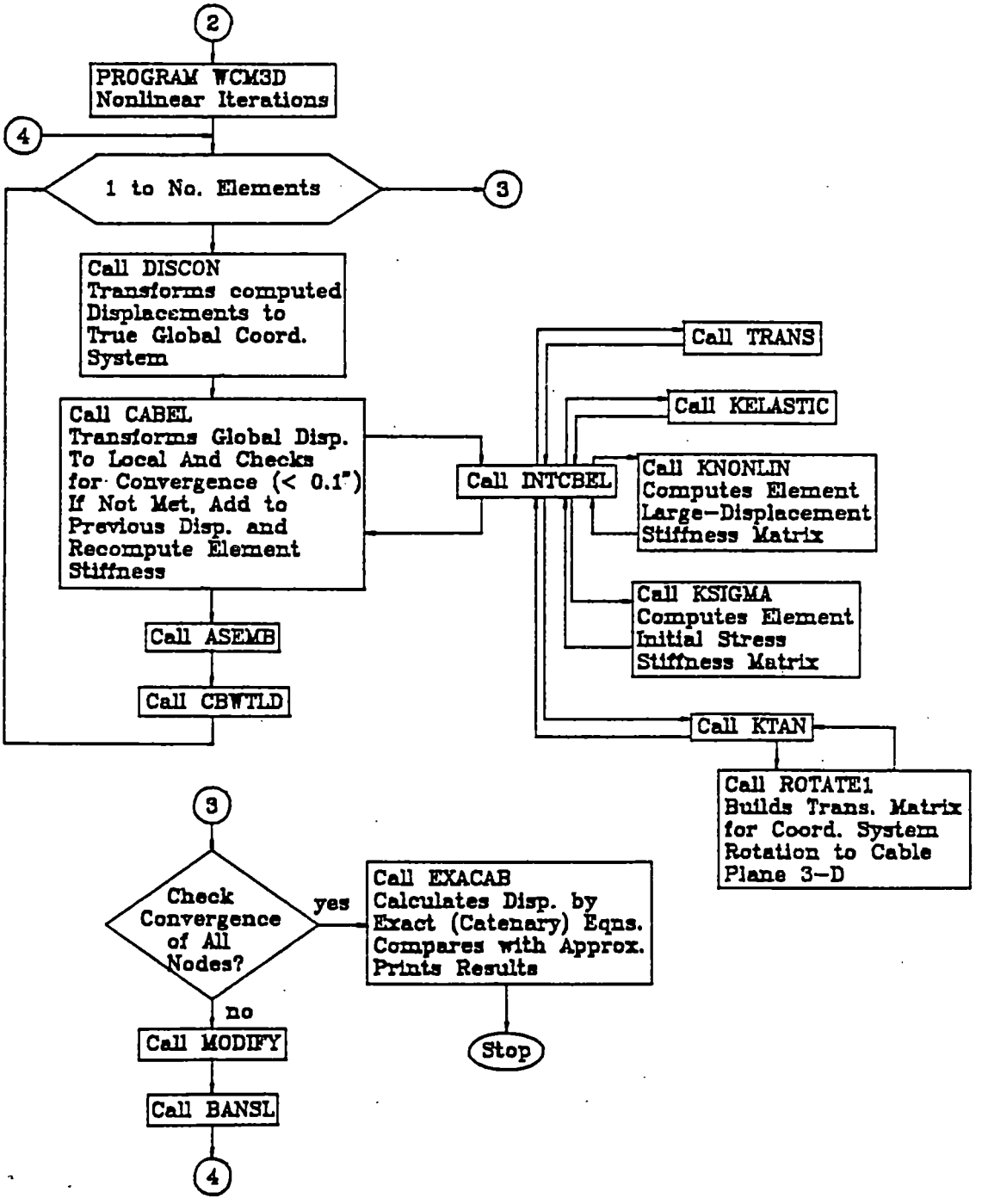

Figure 4.7b CABLE Program Flow Diagram (Nonlinear Analysis)

elongation of a member in tension. Once the linear performance was verified, the program was then tested for modeling a nonlinear cable member. The same sequence of testing was used beginning with cable end points at the same elevation in a principal plane, and ending with an inclined cable being rotated throughout space. Nonlinear results were calibrated through a program feature which compared displacements with exact values. A parametric study was then conducted to investigate element behavior for different tensions, weight, and lengths. Very stiff cables possessing high tension, light weight, and short length were analyzed as well as very flexible cables with low tension, heavy weight, and long length. Number of elements per cable was also explored to verify convergence to the exact solution. The parameter combinations investigated were restricted to realistic values for reasons previously stated. Appendix A presents the results from selected tests to give the reader an understanding of the process.

4.3.2 Study of Moore Creek Bridge Cables

Before constructing the 3–D model of Moore Creek Bridge, a study using CABLE was performed to determine number of elements necessary to model a cable typical of those in the bridge. Figure 4.8 shows cable parameters used for the study. Table 4.1 gives results which shows that four elements per cable were sufficient to accurately approximate the exact cable deformed shape.

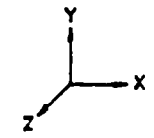

Wt. = 0.018375 k/ft.

$T_{INT} \approx 118.5$ k

E = 23,000 ksi

A = 5.4 $in.^2$

$\Delta Z = -2.56'$

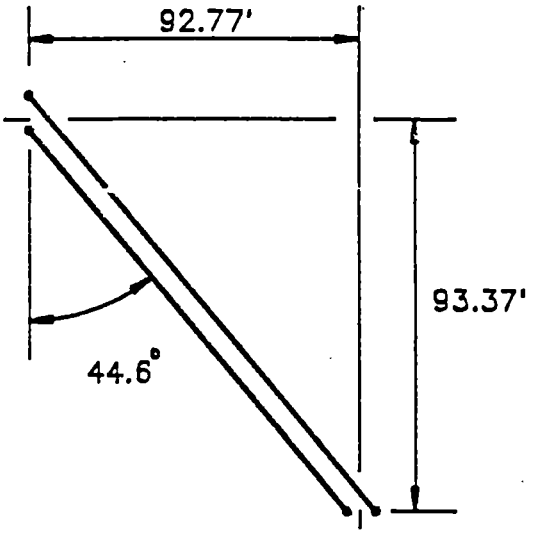

a) Fore–Stays

Wt. = 0.018375 k/ft.

$T_{INT} \approx 182.4$ k

E = 23,000 ksi

A = 5.4 $in.^2$

$\Delta Z = -42.6'$

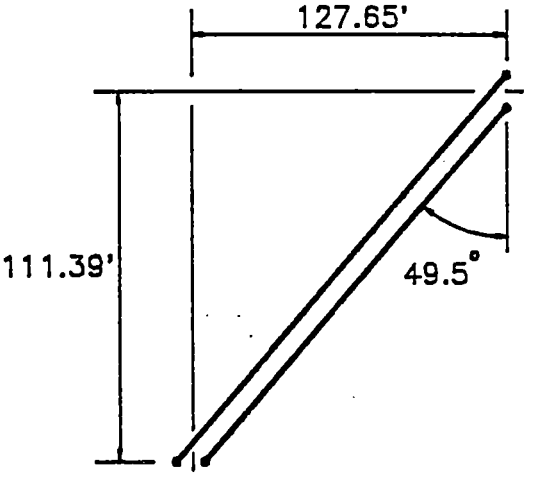

b) Back–Stays

Figure 4.8 Typical Moore Creek Bridge Cables. a)Fore–Stays; b) Back–Stays

Table 4.1 Results of Bridge Cable Parametric Study

Bridge Stay	# of elements per cable	Max % Diff.	Avg. % Diff.
Fore-Stay	2	7.81	3.12
	3	4.53	1.63
	4	3.13	0.92
Back-Stay	3	4.77	1.74
	4	3.34	1.02

Diff. = Difference between computed transverse nodal displacements
% Diff = (Exact - Approx.)/Approx.
Avg. %Diff = Average of absolute difference for all nodes of the cable

5. CABLE–STAYED BRIDGE ANALYSIS PROGRAM

5.1 3–D Finite Element Program

A conventional 3–D finite element program was selected for purposes of investigating behavior of the Moore Creek Bridge. The program utilized 3–D space frame elements (i.e. a 12–DOF two node beam element) before implementing the cable element. In the interest of time, it was decided to combine the entire cable program into the 3–D program instead of adding only the required subroutines. This resulted in using an incremental–iterative type solution process. The process was; cable routines iterated until equilibrium stiffness of the cables were obtained; beam and cable stiffnesses were combined and the entire structure analyzed by the external 3–D routines; cable tensions were then incremented by computed forces in the cable members; total cable forces were sent back into cable routines which iterated to find a new equilibrium stiffness of each cable; the process continued until cable forces no longer changed. To facilitate performing the analysis on a personal computer, an in–core out–of–core solver was incorporated. A brief description of combining the two programs follows.

5.2 Cable Element Integration

5.2.1 Element Compatibility

Special care was exercised to ensure the 3–D space frame program's six degrees–of–freedom (6–DOF) per node elements were compatible with the three degrees–of–freedom (3–DOF) per node cable elements. The 6–DOF per node of the 3–D program elements were translations and rotations in the direction of each global axes. The 3–DOF per node of the cable elements were translations in the direction each of the global axes. DOF compatibility at each node was accommodated by using an ID array. The ID array which identified which DOF existed at that node, was input for each node. Using the ID array, a vector of equation numbers associated with each node was stored. Therefore, it was not

required to distinguish between element types in the input, and compatibility at beam to cable element junctions was maintained.

Although DOF compatibility at cable end nodes was accounted for, in order to be compatible with beam element stiffness, cable stiffness values at these nodes had to be with respect to the global coordinate system. The problem was, in order to restrain cable movement to a single plane, the cable's stiffness at intermediate nodes needed to be with respect to a 3–D system aligned with its plane. In addition, displacements needed for updating cable stiffness and state of stress were required to be consistent with a cable local 3–D coordinate system. To accomplish this, the cable program was modified to perform proper transformations of an element's stiffness matrix if the element was at a cable end. Only portions of that matrix associated with the cable end node was left global. Proper transformations were made to remaining portions so the other two element nodes were in local. This modified stiffness matrix was used in analyzing the structure.

5.2.2 Nonlinear Solution Technique

The cable–stayed bridge analysis program (WCM3D) used an incremental–iteration solution technique. The process was described in section 3.1. Successive cycles of WCM3D computed live load forces in cable members. Within each cycle these forces were added to cable post–tension forces and new cable effective stiffnesses were computed in the cable routines. Convergence was established when cable member forces computed in WCM3D were within a tolerance difference between the current and previous cycles. When total cable forces did not change more than 0.5% from one cycle to another convergence was met. At the point of convergence cable stiffnesses were considered to be in equilibrium with structure forces induced by the loading condition. To ensure convergence and reduce total number of cycles, a relaxation technique was employed when updating cable tensions. The tension used in each cycle to compute a new cable stiffness was an average of total tensions from the last two cycles. The method appeared to reduce the number of cycles for structures with flexible cables but slightly slowed convergence for structures with stiffer

cables. However, when stiff cables were involved, convergence was still achieved within 4–6 cycles. The more flexible a system the more cycles required to reach convergence.

Cable forces computed in each cycle were not calculated by back substitution of nodal displacements into the local force–displacement relations of the cable. Displacements computed in WCM3D were only a change to node position. Total nodal displacements calculated in the cable routines were, therefore, saved and used in Eqns. 4.17, 4.18. and 4.19 to determine each element's current state of stress. Then multiplying by the cable's cross sectional area gave the additional tension force in the cable.

The program WCM3D also possessed the capability of linear analysis. By giving cable members zero initial tension and unit weight, and specifying an elastic analysis, cable nodes were allowed only a single DOF along the local X' axis of the member. No iteration was performed in cable routines and only the elastic stiffness matrix, $\mathbf{K_E}$, was calculated. These elements were then capable of taking compression as well as tension and only a single cycle was required for the solution.

5.3 Program Verification

5.3.1 Studies Conducted

Testing of WCM3D was assisted by the use of a simple frame (see Figure 5.1). Approximately 15 different test cases were analyzed. Frame #1 of Figure 5.1a was initially analyzed without any cables included. This study was used to verify the validity of the space frame analysis portion of the program. Results were confirmed with an exact solution by the moment area method. A cable element was next added (member #4 in Figure 5.1b) at a diagonal across the frame. Assuming the member weightless and without tension, an elastic analysis was performed. Results were confirmed using another 2–D linear finite element analysis program. Next, the cable was given weight and initial tension. Since no other available program had nonlinear capabilities, these results could not be confirmed. However, computed nodal displacements and member forces were examined and determined to be commensurate with hypothesized results for a more flexible member.

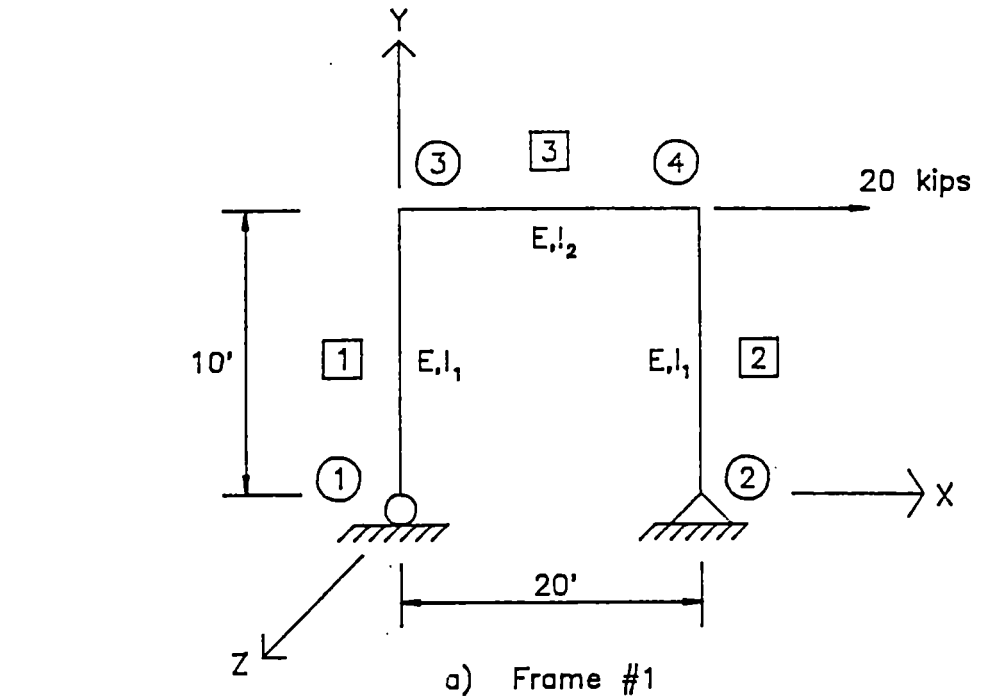

a) Frame #1

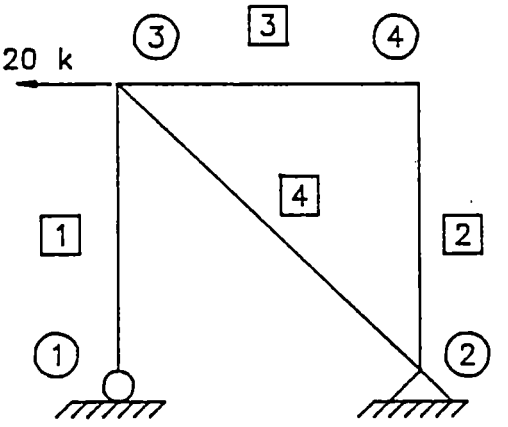

b) Frame #2

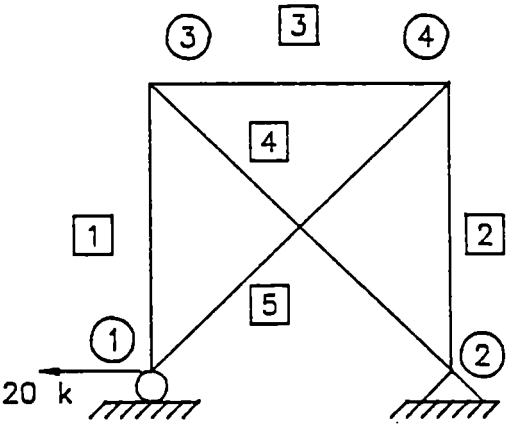

c) Frame #3

Where: $E = 30{,}000$ ksi
$I_1 = 200$ in.^{4} , $A_1 = 100$ in.^{2}
$I_2 = 400$ in.^{4} , $A_2 = 50$ in.^{2}

□ – Element No. ○ – Node No.

Figure 5.1 Program WCM3D Test Frames. a) Frame #1; b) Frame #2; c) Frame #3

To check various program functions, several calibration runs were made varying number of elements per cable and cable stiffness. Final verification tests for frame #2 involved a convergence study of nonlinear to elastic solutions. Initial cable tension was steadily increased while all other components remained the same as the elastic test. Figure 5.2 describes the cable parameters and shows the study results. Based on an examination of the horizontal displacement of node #3, it was found that convergence to the elastic solution was achieved as the initial cable tension increased. As a final test, an additional cable member was added to the frame (see Figure 5.1c). Cable stiffnesses were different and number of elements per cable varied with results being consistent with expected. These frames were also used to test the program's feature of handling either nodal point loads or member concentrated loads. Appendix B provides selected results so the reader can understand the process.

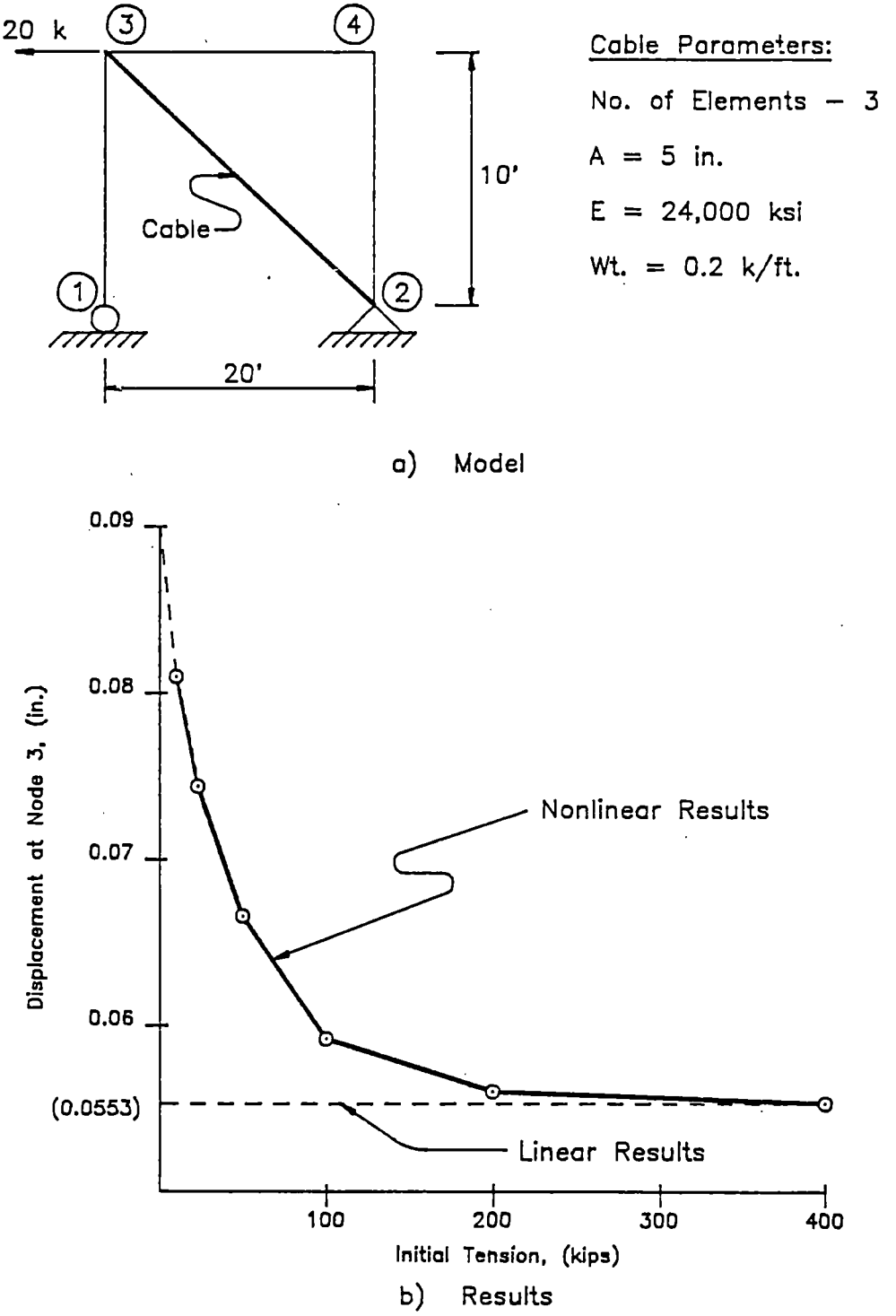

Figure 5.2 Convergence Study of Nonlinear to Linear. a) Model; b) Results

6. MOORE CREEK BRIDGE 3–D ANALYSIS

It was mentioned at the beginning of this report that this research was a continuation of previous studies investigating static behavior of Captain William Cooper Moore Creek Bridge. Previous investigations raised some interesting questions which this research sought to answer.

1. Are assumptions common to a two–dimensional analysis valid for this bridge?
2. Is a three–dimensional analysis necessary to gain an understanding of how this bridge behaves?
3. What loading conditions should be examined and how should they be applied?
4. How is the load distributed, and is the distribution effected by cable nonlinearities?
5. To what extent do cable geometric nonlinearities influence the state–of–stress of this bridge?
6. With cables being post–tensioned, can their behavior be sufficiently approximated by linear elastic assumptions?

It was determined the logical means to attempt to answer these questions was to conduct a 3–D finite element analysis including cable geometric nonlinearities. Since the bridge had been field instrumented and experimentally tested (Hulsey, Delaney, and Briggs(1990)), the data collected provided a mechanism for evaluating the significance, if any, of this type of analysis. Assumptions could be evaluated and limitations found. Therefore, the experimental data provided a datum for comparisons made and a basis for conclusions drawn.

A 2–D linear finite element analysis was previously conducted on Moore Creek Bridge with analytical results compared to experimental (Hulsey and Delaney(1990)). The model finally adopted for analyzing the bridge resulted from several pilot studies surrounding specific features of the bridge's design. Those findings were incorporated in a 3–D model used in this study. The 2–D and 3–D models, analysis details, and comparison results are presented in following sections.

The loading conditions selected to be used in the 3–D study were only a few of those used in the 2–D analysis. Comparison of two–dimensional analytical results with experimental data left little room for improvement when the loads were place symmetrically with respect to the bridge center line. Larger discrepancies were found for loadings asymmetrically placed on the bridge. A total of 12 loading positions with the 160,000 lb. ore trucks (B–Trains) were studied in the 2–D case. Three of which were placed symmetrically on the bridge and the remainder were eccentrically positioned. Six load cases were selected for this 3–D analysis. These were three symmetric and three of the eccentric load cases. The asymmetric loadings selected were B–Trains in the left lane at three positions longitudinally along the bridge. Actual load application and findings of a load distribution pilot study are presented later.

6.1 Cable–Stayed Bridge Analysis History

Cable–stayed bridges are based on the idea that high strength cables can be used instead of piers to support bridge girders and thus provide for long free spans. This provides a complex system with a high degree of indeterminacy combined with nonlinear behavior.

Cable–stayed bridge nonlinearity may be produced by three sources. These are primarily due to: a) large displacements; b) bending moment–axial force interaction; and c) cable drape producing a catenary cable shape (Trotski(1988)).

Numerous analytical methods have been proposed by previous investigators. Some of these methods only account for linear behavior where others have attempted to account for nonlinear effects of the system. The following paragraphs provide a review of the work presented to date by other investigators.

B.E. Lazar (1972) suggested a two–dimensional planer analysis based on a stiffness approach to analyze the behavior of cable–stayed bridges, while M.C. Tang (1971) developed a modulus reduction method (or transfer–matrix method) to evaluate the behavior of

a cable–stayed bridge. Both of these authors suggested an iterative linear elastic analysis procedure for predicting nonlinear behavior of cable–stayed bridges.

Y.C. Loo and S. Srivanich (1983) proposed a method based on the use of an equivalent planer system analysis to determine cable forces and a three–dimensional finite strip analysis to study main stiffening girders. Depending on the technique used to find cable forces, this method provided the opportunity to describe nonlinear cable behavior. The method is only applicable to bridges with single–plane cable arrangements in combination with a single or multiple cell box girder.

M. Como, et al.(1985) examined the static behavior of long span cable–stayed bridges with cables in a fan scheme arrangement. The study focused on the prevailing truss behavior of the bridge through the use of a continuous model and basic statics equations. The method was used since the physical behavior of the fan–shaped scheme is similar to that of a truss. That is, the main state–of–stress is axial in the stays and girder. Girder bending was considered to be a secondary concern. This analysis provided a "truss solution" for the cable elements of the bridge and local bending effects for the girder.

Crawford and Loris (1984) presented a three–dimensional finite element model composed of beam, truss, and cable elements to describe the Brooklyn Bridge. The bridge is a combination suspension and cable–stayed system. The finite element model consisted of approximately 6,000 nodes and 23,000 elements and was used to analyze various rehabilitation strategies.

H. Nakai, et al.(1985) developed an analytical method for analyzing the elasto–plastic and finite displacement behavior of a cable–stayed bridge during the erection stages up to completion. The method was based on the use of a three–dimensional model which consisted of a straight box girder and cable elements to determine the ultimate strength of the bridge. Cable nonlinearities and nonlinearities induced by element deformations were accounted for.

The use of models to investigate prototype behavior of cable–stayed bridges has been employed on numerous occasions. Models have been used to confirm analytical results, analyze questionable construction phases or techniques, and predict the nonlinear performance of cable–stayed bridges (Kayser and Binkhorst(1975); Koizumi et al.(1985); Trotski and Lazar(1971)).

R. Das (1976) developed a procedure for the design of stiffening girders for a cable–stayed bridge. An iterative method to account for large displacements using the finite element method was used to explain the transfer of cable forces to the main girder. N. Gimsing (1976) examined the behavior of multi–span cable–stayed bridges. the study focused on pylons of inner cable systems which were not horizontally fixed by cables connected to piers or abutments. The results showed that unacceptable stiffening girder deflections can occur or massive pylon cross–sections are required. Alternate pylon designs alleviating these problems were discussed and suggested.

Most available research to date is either limited in its applicablility to single–plane cable configurations or two–dimensional planer systems etc., or methods have been developed for specific configurations such as the single or multiple cell box girder type cable–stayed bridge (Loo and Srivanich(1983)). The analytical results reported in the literature for box girder type bridges with orthotropic steel decks have generally focused on membrane stresses and local bending moments in the steel box girder.

In addition to longitudinal and local bending of the plates that comprise a box girder, eccentric loads induce torsional bending which must be accounted for in the analysis. Therefore, analytical methods are needed to account for the three–dimensional interaction of the nonlinear behavior of cables and effects of eccentric loading. Traditional two–dimensional plane frame or three–dimensional space frame programs to not satisfy this need.

The literature review illustrates that cable–stayed bridges previously investigated transfer load between girders through the torsional rigidity of the deck in the following manner:

a) through the use of an orthotropic steel deck; or

b) through transverse stiffening girder diaphragms.

The manner in which applied loads were distributed from the deck to the members was not found in the literature for cable–stayed systems. Primarily discussion focused on: a) type of structure and variables investigated; b) modeling techniques employed; c) analytical methods used; and d) results or findings. The method of distributing loads, their magnitudes and points of application, may significantly effect analysis results. If load distribution can be accurately determined a simpler modeling technique may prove to be just as efficient as a more sophisticated technique. A 2–D model can give results just as accurate as a 3–D if the proper loading is applied. However, load transfer mechanisms of most structures are not simple and extra studies may be necessary just to predict an appropriate loading scheme.

6.2 Moore Creek Bridge Details

Captain William Cooper Moore Creek Bridge is a unique cable–stayed bridge for four reasons. These are: a) the clear span of the structure is very short; b) the girder–pylon bearing support interface is very unusual; c) the load transfer between girders is obtained through floor beams connected to the main girders by shear type web plates; and d) the structure experiences light traffic volumes but unusually heavy loads and harsh environmental conditions.

The bridge has a timber deck supported by floor beams which provide an unknown amount of interaction between girders. That is the floor beams are connected to the main girder by web plates (see Figure 1.1). Thus, based on the assumption that web plates transfer little–to–no moment (shear connection), it may be said that a precise piece–wise investigation of the individual girders is not necessary to gain an understanding of the

girder member stresses and displacements. The shear connections, however, influence load transfer from floor beams to girders. Being neither a rigid fixed connection nor free to rotate as a pinned connection the amount of moment transfer is unknown. Load distribution to the floor beams themselves could be effected by plate action of the timber deck. To investigate cable nonlinearities and rigidity of the deck system along with reasons previously stated a three–dimensional finite element analysis (Zienkiewicz(1981)) including cable geometric nonlinearities was used for the analysis presented in this report.

6.3 Analytical Models

6.3.1 Two–Dimensional Model

The final 2–D model used in a previous investigation evolved from two parametric studies therein conducted: 1) Study of boundary conditions surrounding prestressed rock anchors; and 2) Investigation of the behavior of the girder–to–pylon bearing support. The reader is referred to Hulsey and Delaney (1990) for specific details of the analysis. Figure 6.1 shows the final model used in that study. Six DOF beam elements were used for all member except the cables. For the cables a single linear two–node 2–DOF axial element was used. The model contained a total of 68 nodes and 70 elements.

Record of load position during the experimental tests was made in reference to the bridge deck floor beams and distance from the left guardrail when facing up station. With nodes located along the girders at each floor beam to girder connection, correlation between load position number and where to place nodal point loads on the model was made as shown in Figure 6.2. These same load position numbers will be used to described loadings for the 3–D analysis later in this report.

6.3.2 Three–Dimensional Model

In the 2–D study a separate model had to be constructed for each side of the bridge. This was because a slight elevation difference existed between some of the supports from one side to another. The global coordinate system for the 3–D study was located with

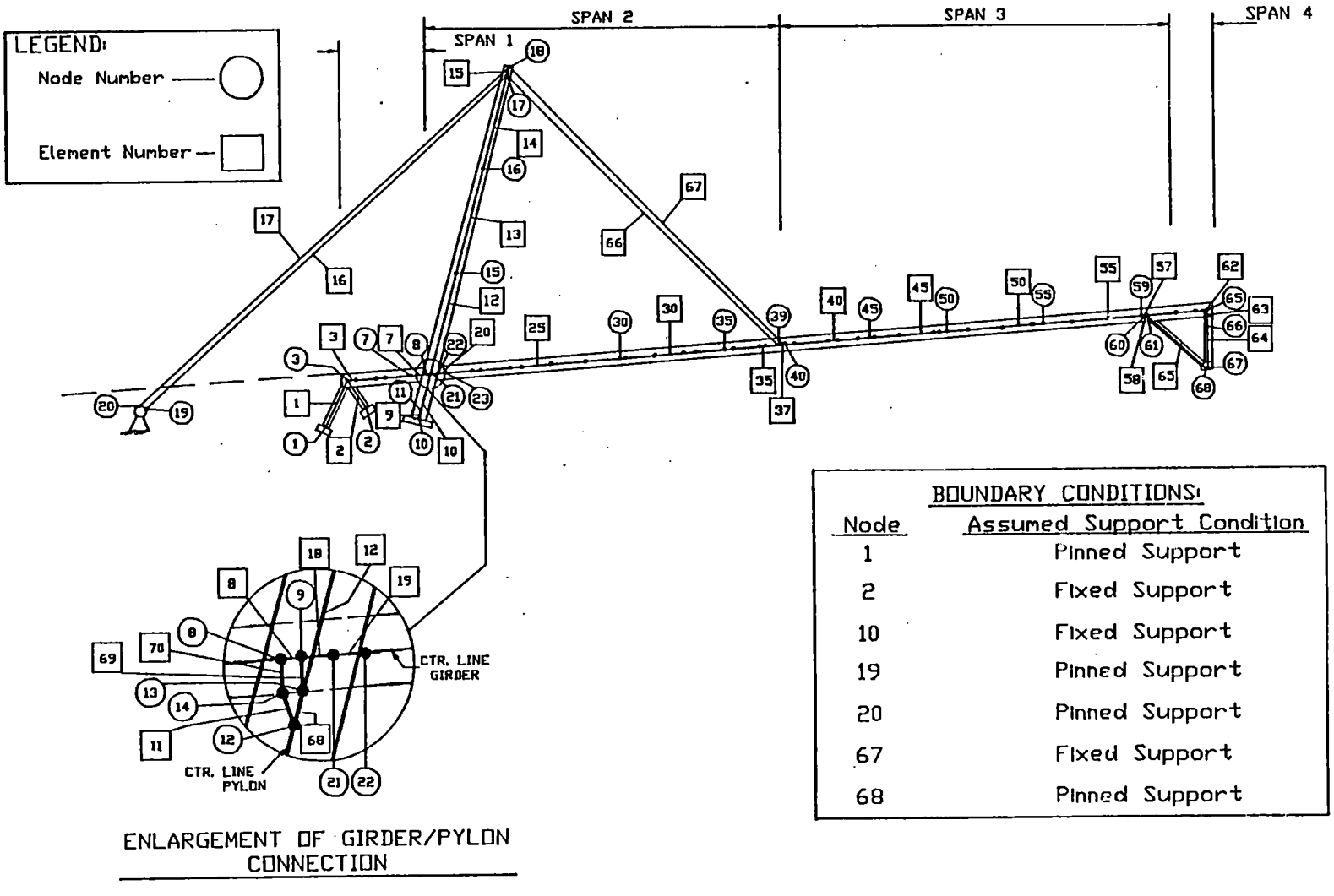

BOUNDARY CONDITIONS:

Node	Assumed Support Condition
1	Pinned Support
2	Fixed Support
10	Fixed Support
19	Pinned Support
20	Pinned Support
67	Fixed Support
68	Pinned Support

Figure 6.1 2-D Finite Element Model

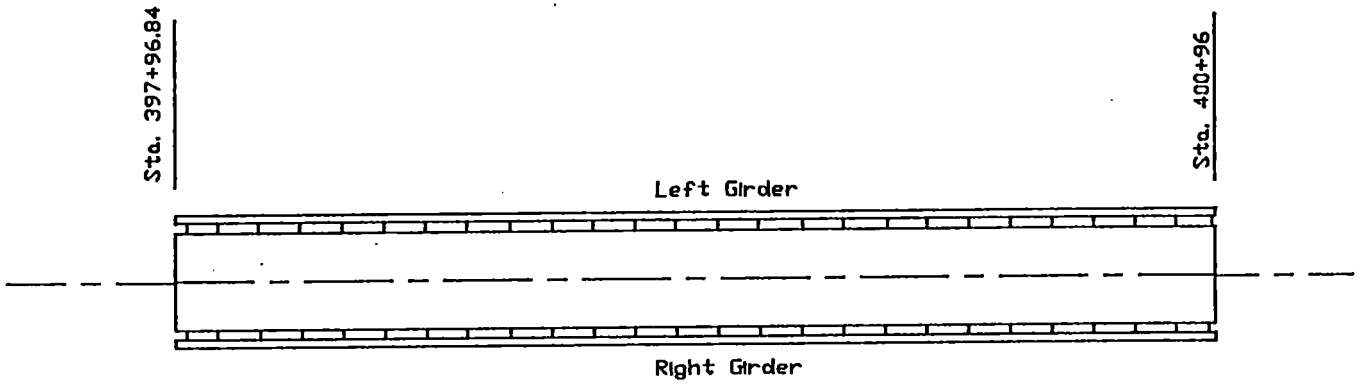

BRIDGE DECK PLAN VIEW

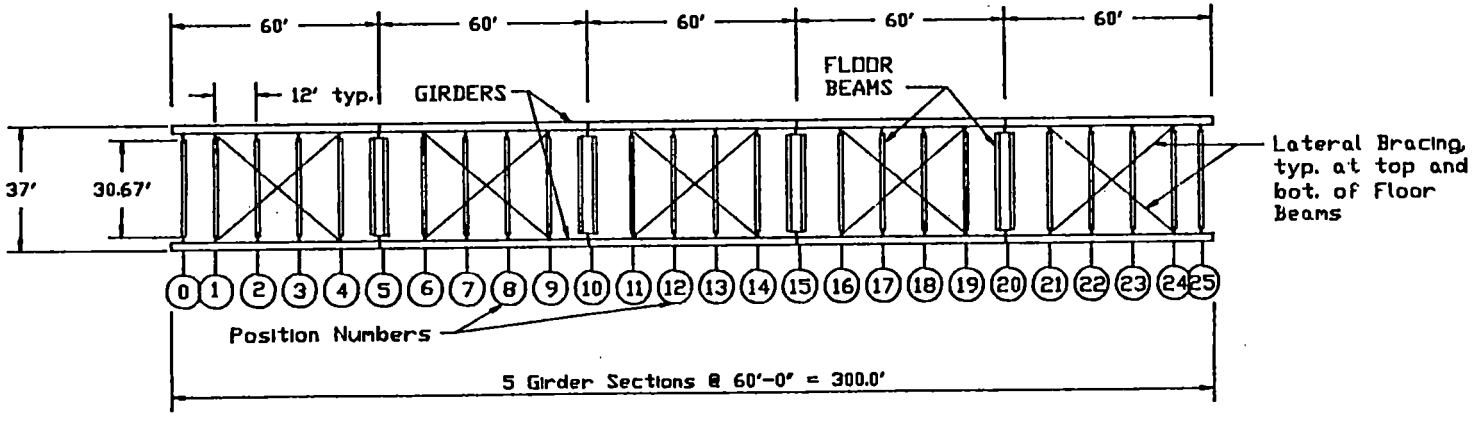

BRIDGE FRAME PLAN VIEW

Figure 6.2 Bridge Frame and Floor Beams

the X axis coinciding with the bridge center line, vertical Y axis was positive upward, and Z axis horizontal and positive outward. Because of the bridge's symmetrical design, construction of the 3–D model was a simple task of connecting opposite sides of the 2–D model with floor beams, cross bracings, etc. Therefore, the 3–D model is a consistent extension of that used in the 2–D analysis (see Figure 6.3). The only exception being how the cables were modeled. As described in Section 4.3.2 a parametric study was conducted using the program CABLE to determine the optimum number of elements necessary to model cables of Moore Creek Bridge. It was found that four elements were sufficient. Thus, four nonlinear three–node elements were used for modeling each cable. A total of 194 nodes and 214 elements were used. This gave 924 equations with a bandwith of 304.

Element section properties for the 2–D analysis were determined from actual construction plans of the bridge and were also used in the 3–D analysis. Properties of additional elements needed only in the 3–D analysis were also obtained from the bridge plans. Table 6.1 shows the properties used and a description of where they occur.

6.4 Static Loading Conditions

Load conditions selected for this analysis were taken from loadings used in the experimental investigation. A total of six of the B–Train loadings were used, three in the bridge's left lane and three on the center line. B–trains were approximately 160,000 lb. ore trucks traveling from the Yukon Territory in Canada to Skagway, Alaska.(see Figure 6.4) Axle weights for each truck used were obtained by weighing at a nearby weigh station. For the loading conditions selected, two separate B–Trains were used, one for the symmetric loadings and one for the eccentric loadings, with total weights of 157.55 kips and 157.37 kips respectively. The trucks were placed statically at three positions longitudinally along the bridge (see Figure 6.5).

For the purposes of nomenclature, the loadings will be referred to as Case 1–6. Cases 1, 2, & 3 are with B–Train #216 in left lane at positions 4, 9, & 14 respectively (see Table 6.2). Cases 4, 5, & 6 are with B–Train #204 on center line at positions 4, 9, & 14

Table 6.1 Section Properties (3-D FEA)

Prop No	X-Sect. Area(in^2)	Ixx (in^4)	Iyy (in^4)	Izz (in^4)	Description
1	83	28604.1	12133.	52662.2	Original Girder
2	130	31252.12	15181.	94131.3	Girder w/ Plates
3	130	31285.3	15452.	95429.8	Girder w/ Plates
4	120	30831.3	16376.	83897.5	Girder @ Cables
5	120	30892.2	13580.	85015.3	Girder w/ Plates
6	120	31035	14085.	88411.5	Girder w/ Plates
7	290	70000	27297.	99012.35	Girder Concrete Filled
8	200	117429.3	99577.	92869.1	Cables
9	91	24960.02	16321.	45454.4	Pylon Base
10	87	22707.3	15391	38550.8	Pylon Base to Taper
11	79	18534.5	13530.	32290.5	Lowest Upper Pylon Section
12	71	14478.1	11669.	17536.5	Middle Upper Pylon Section
13	81	7450.7	59603.	59603.6	Top Upper Pylon Section
14	28	3884.6	31076.	31076.78	Concrete Filled Column
15	62	575.98	41924.	11325.9	Floor Beams
16	43	4705.5	731.5	1453.03	Strut
17	0.79	0.01	0.01	0.01	Cross-Bars
18	6.8	0.01	0.01	0.01	Cross-Bracing
19	2400	0.01	0.01	0.01	Elastomeric Bearing Pad
20	1000	0.01	0.01	900000	Girder Center to Bottom
21	1000000	0.01	999999	0.01	Curved Steel Plate

Table 6.2 Loads for B-Train #216 in left lane

Axle Position	Load (kips)
Front Axle -	12.225
1st Tandum -	41.563
Lone Axle –	21.322
2nd Tandum -	41.344
3rd Tandum -	40.925
TOTAL	157.379

Case #1 $B = 52.5$ in. Position #4		Case #2 $B = 50.5$ in. Position #9		Case#3 $B = 50$ in. Position #14	
Node No.	Girder Loads (k)	Node No.	Girder Loads (k)	Node No.	Girder Loads (k)
79	-2.702	93	-2.643	141	-2.630
80	-9.523	94	-9.582	142	-9.597
83	-6.047	97	-5.920	147	-5.882
84	-21.314	98	-21.450	148	-21.479
85	-3.659	99	-3.584	151	-3.559
86	-12.897	100	-12.980	152	-12.997
87	-5.301	103	-5.158	153	-5.156
88	-18.684	104	-18.81	154	-18.83
89	-6.853	139	-6.703	159	-6.665
90	-24.155	140	-24.305	160	-24.334
93	-1.174	141	-1.148	161	-1.142
94	-4.137	142	-4.163	162	-4.169
97	-2.714	147	-2.654	167	-2.639
98	-9.564	148	-9.623	168	-9.638
99	-6.332	151	-6.193	169	-6.159
100	-22.316	152	-22.454	170	-22.489
Totals:	-157.372		-157.370		-157.365

Table 6.3 Loads for B-Train #204 on Center Line

Axle Position	Load (kips)
Front Axle -	12.071
1st Tandum -	41.256
Lone Axle –	21.982
2nd Tandum -	41.652
3rd Tandum -	40.595
TOTAL	157.556

Case #4 $B = 168$ in. Position #4		Case #5 $B = 168$ in. Position #9		Case#6 $B = 168$ in. Position #14	
Node No.	Girder Loads (k)	Node No.	Girder Loads (k)	Node No.	Girder Loads (k)
79	-6.036	93	-6.036	141	-6.036
80	-6.036	94	-6.036	142	-6.036
83	-13.579	97	-13.579	147	-13.579
84	-13.579	98	-13.579	148	-13.579
85	-8.262	99	-8.262	151	-8.262
86	88.262	100	-8.262	152	-8.262
87	-12.305	103	-12.305	153	-12.305
88	-12.305	104	-12.305	154	-12.305
89	-15.62	139	-15.62	159	-15.62
90	-15.62	140	-15.62	160	-15.62
93	-2.675	141	-2.675	161	-2.675
94	-2.675	142	-2.675	162	-2.675
97	-6.089	147	-6.089	167	-6.089
98	-6.089	148	-6.089	168	-6.089
99	-14.208	151	-14.208	169	-14.208
100	-14.208	152	-14.208	170	-14.208
Totals:	-157.548		-157.548		-157.548

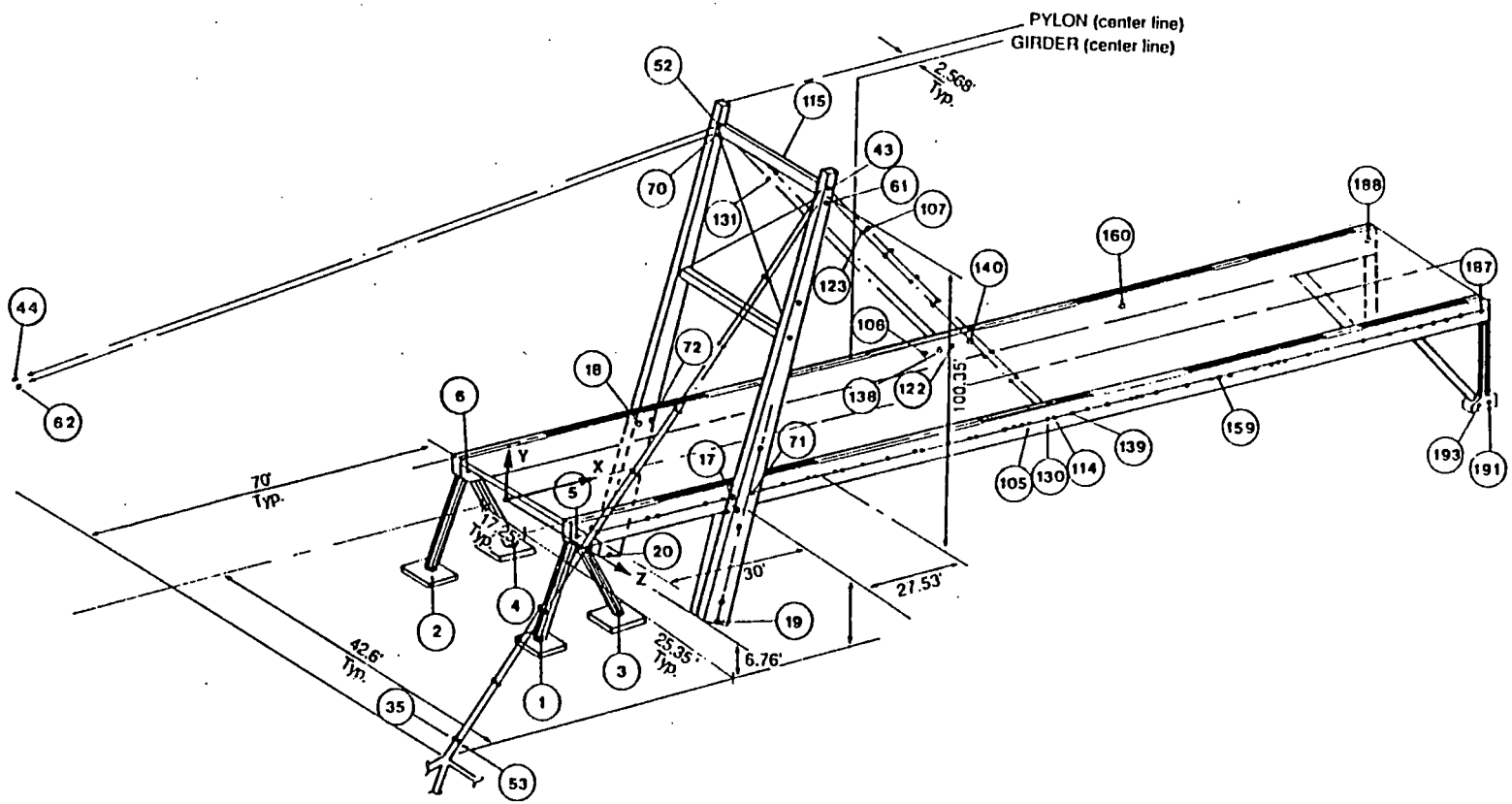

Figure 6.3 3-D Finite Element Model

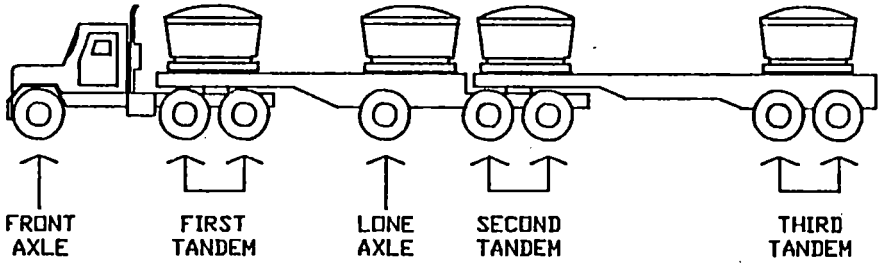

SIDE VIEW

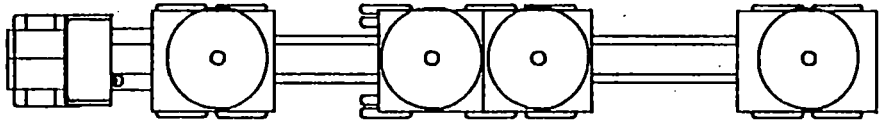

TOP VIEW

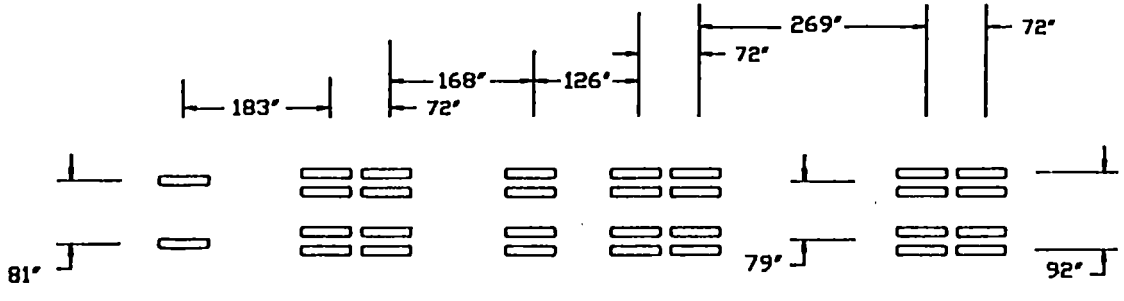

TIRE FOOTPRINT

Figure 6.4 Ore Truck configuration (B-Train)

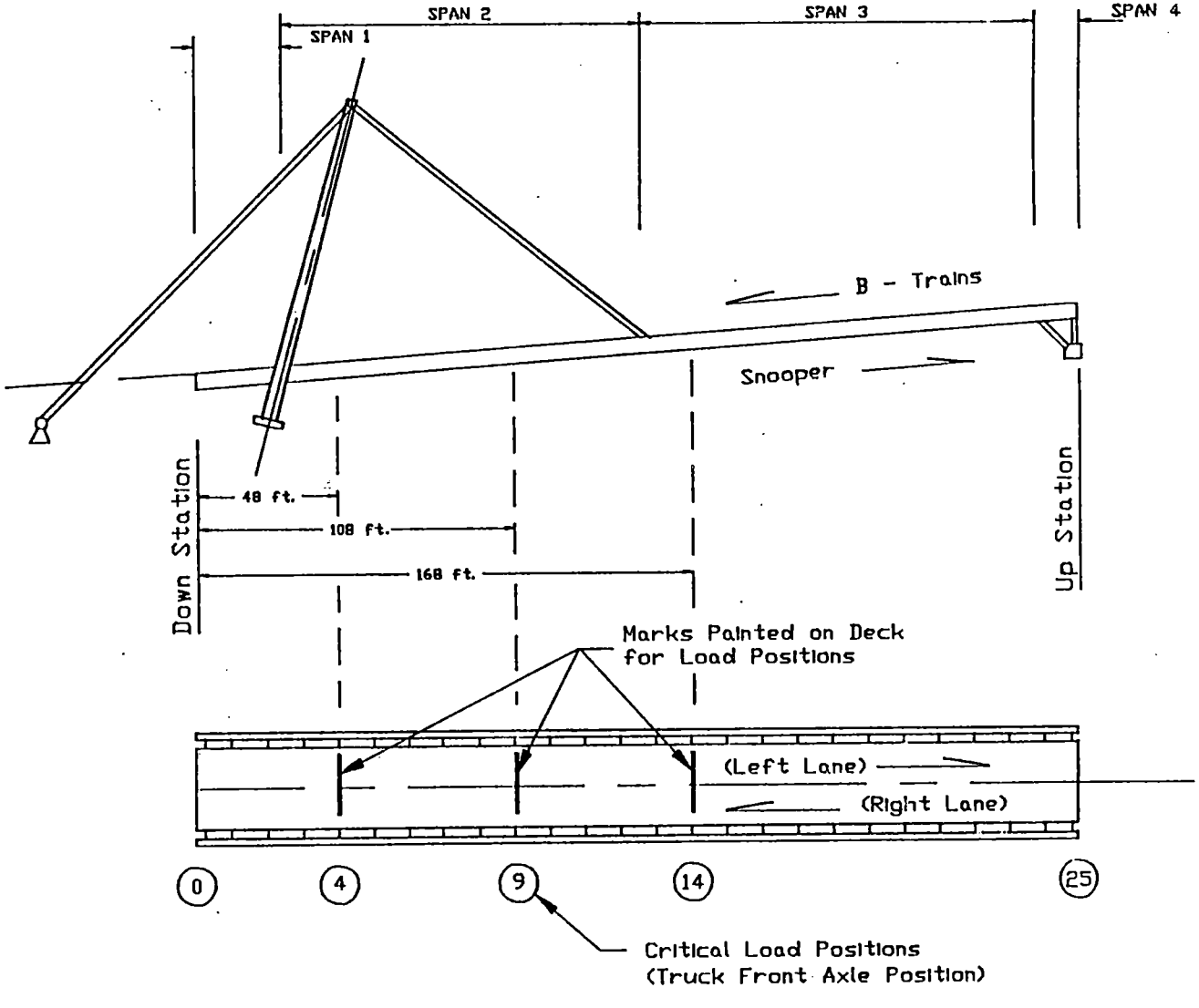

Figure 6.5 Bridge Frame and Critical Load Positions

respectively (see Table 6.3). Reference in the tables to a distance B implies the transverse distance from truck's center line to the face of left guardrail. In order to make a consistent comparison between modeling techniques the same load distribution technique used in the 2–D analysis was used for the 3–D analysis. Axle location with respect to floor beams was used to distribute loads to the appropriate beam. These beam loads were then distributed to the girders assuming pinned connections and reaction forces used as nodal point loads applied to the girders. Results of a pilot study investigating the validity of this method of load distribution follows this section.

6.4.1 Load Distribution Pilot Studies

Before analyzing Moore Creek Bridge three–dimensionally, assumptions about how loads were to be applied were investigated. For the 2–D analysis, principals of statics were used. First, assuming the timber deck to be a simply supported beam, axle loads were transferred to the floor beams. Second, assuming floor beams to be simply connected to girders, loads were transferred to girders and applied as concentrated nodal point loads on the 2–D frame. This technique is common to 2–D analysis. Since the 3–D model contained the floor beams and it was thought the shear type fasteners used to connect floor beams to girders offered some moment transfer, a series of analyses were conducted. Six different cases were investigated where the load was applied and a complete analysis of the bridge performed. Variables influencing load distribution examined were: a) floor beam stiffness; b) floor beam to girder connection; and c) timber deck.

Loading case #2, with the B–Train in left lane at approximately the bridge's longitudinal mid point, was used for the pilot study. Maximum girder deflection was used for comparison purposes. Experimentally, the maximum deflection measured for this loading was -2.76 inches for the left girder and -1.68 inches for the right. The 2-D analysis predicted a maximum of -3.40 inches and -0.94 inches for the left and right girders respectively. Table 6.4 shows the 3–D analysis results for each test. The details of the tests follow.

Table 6.4 Load Distribution Pilot Study Results

Test Case	Bm./Gdr. Interface	Beam		Deflection(in)	
		(Izz)	(Ixx)	Lt. Girder	Rt. Girder
Experiment	—	—	—	-2.76	-1.68
2–D	Pinned	—	—	-3.4	-0.94
3–D					
2F	Fixed	8948	8.25	-3.89	-0.5
2IF	Fixed	11325	575	-3.84	-0.56
2IP	Pinned	11325	575	-3.25	-1.15
2IPF	Hinged	11325	575	-3.32	-1.07
2IPJ	Pinned	11325	999999	-2.28	-2.11
2IPF	Fixed	11325	999999	-2.33	-2.06

Influence of floor beam stiffness was first investigated. Case 2F consisted of giving each beam a moment of inertia about its strong axis, I_{zz}, and polar moment about its longitudinal axis, I_{xx}, that only of the beam itself (see Figure 6.6a). Then for Case 2IF the timber deck and beam were considered as a composite section. It was assumed only the tributary width of the deck, based on a 12 ft. beam spacing, contributed to the stiffness (see Figure 6.6a). For both cases, the loading assumed was member concentrated loads distributed to member ends using fixed end relationships. Results showed that deflections were over predicted for the left girder and under predicted for the right girder. Beam stiffness had a minor affect on load distribution.

In conjunction with Case 2IF described above, two other methods of distributing loads to floor beam ends were examined. Case 2IF assumed fixed end conditions, Case 2IP assumed pinned conditions, and Case 2IPF assumed hinges at the web plates (see Figure 6.7). For all cases, I_{zz} and I_{xx} included the deck as described above. In order to thoroughly investigate the connection behavior an additional node could be placed where the internal hinge was located and connected to a rotational spring. Then spring stiffness could be varied to investigate moment transfer of the connection. This was not done here because this was only a pilot study external to the intent of the project. These studies showed a significant difference between fixed end and pinned end assumptions. Results for pinned end connections showed improvement over 2–D results. In all cases, however, computed left girder displacements were still larger than experimental and computed right girder displacements were still smaller.

The above studies indicated plate action coupled with beam stiffness and floor beam connections may influence the load distribution to the girders. To develop a better understanding of the load distribution, a plate element could be incorporated in the finite element program to model the timber deck. Rotational springs could also be connected at the floor beam to girder connection nodes to allow a variable rotational resistance. Another suggested technique would be to use a plate program to model the deck system

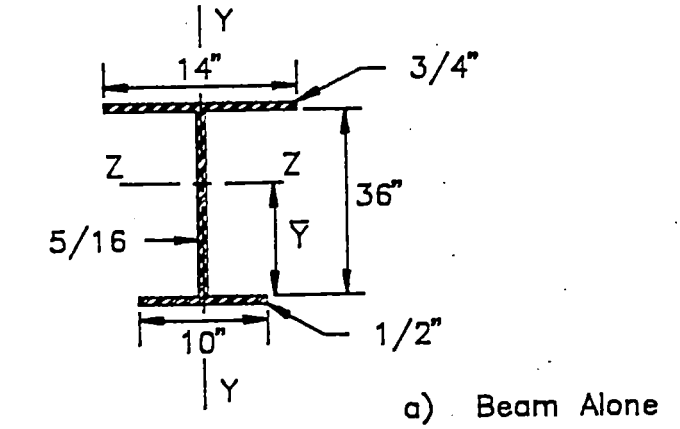

$\bar{Y} = 25.94$ in.

$A = 23$ in.^{2}

$I_{zz} = 8{,}948$ in.^{4}

$I_{xx} = 8.25$ in.^{4}

$$n = \frac{E_w}{E_s} = \frac{1{,}200}{29{,}000}$$

$n = 0.01438$

$A_E = 61.51$ in.^{2}

$I_{zz_E} = 11{,}326$ in.^{4}

$I_{xx_E} = 576$ in.^{4}

$\bar{Y} = 32.73$ in.

(E = Effective for Steel)

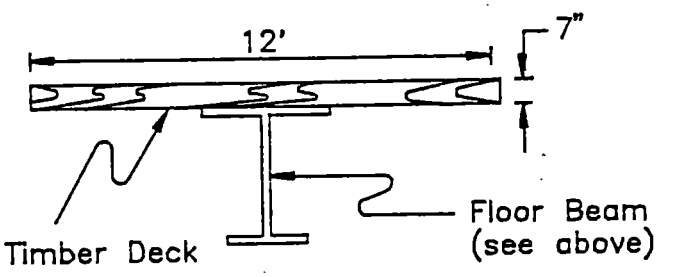

b) Beam–Deck System

Figure 6.6 Floor Beam Properties. a) Beam Alone; b) Beam–Deck System

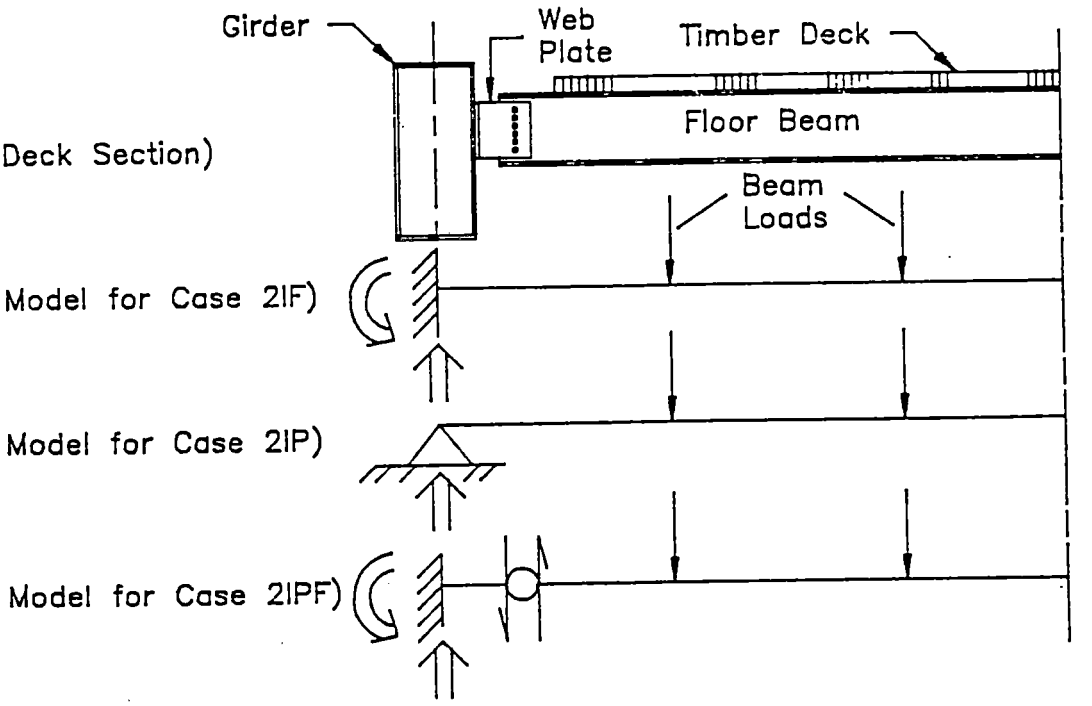

Figure 6.7 Floor Beam To Girder Connection Models

and insert axial springs at the floor beam ends. Determining spring forces at beam–girder connection points as a result of the applied loads would give girder nodal point loads for a space frame analysis. Because this was only a pilot study and not an emphasis of the research, these methods are only suggested for possible further studies. To bound the problem, the deck was made rigid by giving the floor beam elements an infinite rotational resistance ($I_{xx} = 999999in^4$). Case 2IPJ, with a pinned end load distribution, and Case 2IFJ, with a fixed end load distribution, were examined. Results showed deck stiffness did indeed effect the load distribution. Girder deflections leveled out approaching the magnitudes measured in the field, but assuming total rigidity of the timber deck was neither accurate nor justifiable. A more detailed analysis of the deck action itself would be required to determine an accurate measure of its stiffness.

This pilot study confirms that proper distribution of loads in the Moore Creek Bridge is effected by a combination of timber deck plate action and web plate connection rigidity. Further investigations should be conducted to explore the extent of their impact.

6.5 Analytical Results

The Captain William Cooper Moore Creek Bridge, located near Skagway, Alaska, was analyzed for static loading conditions. A three–dimensional finite element program consisting of space frame beam elements and nonlinear three–node axial elements was used for the analysis. The nonlinear elements were used to model the cable–stays and investigate their geometric nonlinear influence in the bridge's behavior under static loads. Previous to this investigation, this bridge was tested experimentally through field instrumentation and testing under actual bridge loads. The experimental study was followed by a 2–D finite element analysis with the bridge subjected to the same loads as those used in the field.

For the 3–D analysis, six loading cases involving B–Trains weighing approximately 160,000 lb. were investigated. These loads consisted of: a) a truck placed eccentrically with respect to the bridge's longitudinal center line at three positions along its length;

and b) a truck centered on the bridge's center line at three longitudinal locations. Loads applied to the structure in the 3–D analysis were distributed consistent with the manner in which they were distributed in the 2–D study to provide for a valid comparison of modeling techniques. Findings from the load distribution pilot study presented in Section 6.4.1 show the transfer of load from the point of application to the girders is effected by deck plate action and the web plate shear connections. It was beyond the scope of this research to perform a more sophisticated analysis of load distribution and it is recommended that future investigations of this bridge begin with such a study.

Results of the 2–D study indicated the bridge's three–dimensional behavior should be investigated. The following sections present results of the 3–D finite element analysis and a comparison made with both the experimental and 2–D results.

6.5.1 Girder Deflections

The purpose of this study was to gain insight into the behavior of the cable–stayed Moore Creek Bridge and attempt to answer questions raised by previous investigations of said bridge. Under symmetric loading conditions, a 2–D analysis, when compared to experimental data, proved sufficient for predicting girder deflections. When asymmetric loads (lane loads) were applied, the comparison of 2–D findings with experimental data showed a consistent over prediction of deflections for the girder nearest the load and under prediction of deflections for the girder on the opposite side. This raised the question of whether the interaction between opposite sides could be accounted for by the assumptions of modeling each side of this bridge individually (2-D assumptions)? Also, is a 3–D analysis capable of improving predictions of girder deflections when the bridge is subjected to lane loads, and are the geometric nonlinearities associated with the bridge's cables significant enough to affect girder deflections under their current post–tension forces?

Figure 6.8 shows the locations of nodes where girder deflections were measured during experimental testing. Computed deflections at these locations in the 2–D and 3–D FEM studies were compared with those measured in the field. The B–Train loadings examined

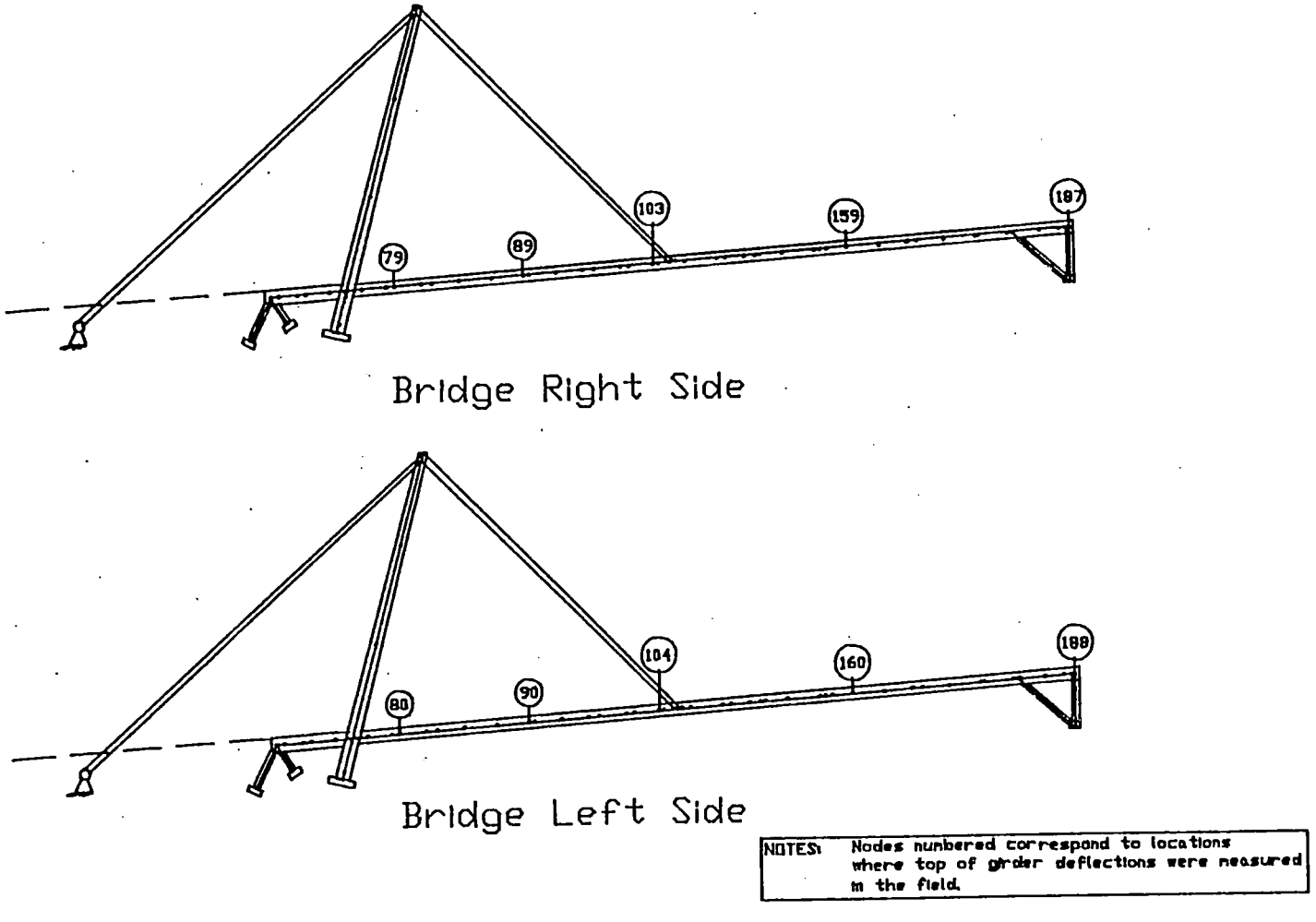

Figure 6.8 FEM Model Showing Nodes for Deflection Study

in the 3–D analysis were: a) a truck located at three positions along the bridge placed asymmetrically with respect to the bridge's longitudinal center line; and b) a truck centered on the bridge center line at three positions along its length. These load cases are described in detail in Section 6.4.

Results of the girder deflection study showed that a nonlinear 3–D analysis did improve the prediction of deflections under asymmetric loading conditions. However, the maximum improvement was only 0.27 inches for the left girder with the B–Train in the left lane at position #14 (Load Case #3). Under a symmetric load, 3–D results and 2–D results were essentially equal with a maximum difference of 0.03 inches.

For the eccentric loadings, the maximum discrepancy between 3–D analytical and experimental values was 0.62 inches over predicted by the model and occurred along the left girder at node 104 with the truck at position #4 (Load Case #1). The maximum vertical deflections predicted by the 3–D model were −2.28, −3.24, and −2.39 inches for the left girder and −0.87, −1.14, and −0.98 inches for the right girder under lane load cases 1, 2, and 3 respectively.

Under symmetric loads, the 3–D analytical results were a maximum of 0.5 inches above the experimental which occurred along the left girder at node 80 with the B–Train at position #4 (Load Case #4). For the symmetric load cases 4, 5, and 6, the maximum vertical deflections predicted by the 3–D model were −1.58, −2.20, and −1.69 inches for the left girder and −1.54, −2.18, and −1.69 inches for the right girder respectively.

Because the results from the 3–D nonlinear analysis and the 2–D linear analysis were essentially equal for symmetric loads, a 3–D linear analysis was performed only for an eccentric loading with a B–Train in the left lane at position #9 (Load Case #2). This test was to investigate the behavioral influence of cable geometric nonlinearities. Results of the 3–D linear test showed a 0.02 inch maximum difference in predicted girder deflections between the linear and nonlinear analysis under load Case #2. Tables 6.5 through 6.8

Table 6.5 Left Girder Deflections Under Eccentric Loads

Load Case	Node No	Deflections (in.)					
			Computed		Deflection Difference		
		Measured	2D	3D	2D (a)	3D (a)	3D - 2D
1	6	0.00	0.00	0.00	0.00	0.00	0.00
	80	-0.36	-0.59	-0.56	0.23	0.20	0.03
	90	-1.80	-2.44	-2.28	0.64	0.48	0.16
	104	-1.44	-2.15	-2.06	0.71	0.62	0.09
	160	-0.36	-0.69	-0.70	0.33	0.34	-0.01
	188	0.00	0.00	0.00	0.00	0.00	0.00
2	6	0.00	0.00	0.00	0.00	0.00	0.00
	80	-0.24	-0.38	-0.37	0.14	0.13	0.01
	90	-2.40	-2.29	-2.18	-0.11	-0.22	0.11
	104	-2.76	-3.40	-3.24	0.65	0.48	0.16
	160	-1.56	-2.11	-1.96	0.55	0.40	0.15
	188	0.00	0.00	0.00	0.00	0.00	0.00
3	6	0.00	0.00	0.00	0.00	0.00	0.00
	80	0.00	-0.12	-0.13	0.12	0.13	-0.01
	90	-0.72	-0.84	-0.86	0.12	0.14	-0.02
	104	-1.44	-2.08	-1.97	0.64	0.53	0.11
	160	-2.04	-2.66	-2.39	0.62	0.35	0.27
	188	0.00	0.00	0.00	0.00	0.00	0.00

a) Difference = Measured - Calculated

b) Difference = 3D - 2D

Note: Max difference is underlined

Table 6.6 Right Girder Deflections Under Eccentric Loads

Load Case	Node No	Deflections (in.)					
			Computed		Deflection Difference		
		Measured	2D	3D	2D (a)	3D (a)	3D - 2D
1	5	0.00	0.00	0.00	0.00	0.00	0.00
	79	-0.12	-0.15	-0.19	0.03	0.07	-0.04
	89	-1.20	-0.68	-0.87	-0.52	-0.33	-0.19
	103	-1.08	-0.60	-0.73	-0.48	-0.35	-0.13
	159	-0.36	-0.20	-0.20	-0.16	-0.16	0.00
	187	0.00	0.00	0.00	0.00	0.00	0.00
2	5	0.00	0.00	0.00	0.00	0.00	0.00
	79	-0.12	-0.10	-0.11	-0.02	-0.01	-0.01
	89	-0.96	-0.63	-0.77	-0.33	-0.19	-0.14
	103	-1.68	-0.94	-1.14	-0.74	-0.54	-0.20
	159	-0.96	-0.59	-0.73	-0.37	-0.23	-0.14
	187	0.00	0.00	0.00	0.00	0.00	0.00
3	5	0.00	0.00	0.00	0.00	0.00	0.00
	79	0.00	-0.03	-0.03	0.03	0.03	0.00
	89	-0.56	-0.23	-0.25	-0.33	-0.31	-0.02
	103	-0.96	-0.58	-0.71	-0.38	-0.25	-0.13
	159	-1.20	-0.74	-0.98	-0.46	-0.22	-0.24
	187	0.00	0.00	0.00	0.00	0.00	0.00

a) Difference = Measured - Calculated

b) Difference = 3D - 2D

Note: Max difference is underlined

Table 6.7 Left Girder Deflections Under Symmetric Loads

Load Case	Node No	Deflections (in.)					
			Computed		Deflection Difference		
		Measured	2D	3D	2D (a)	3D (a)	3D - 2D
4	6	0.00	0.00	0.00	0.00	0.00	0.00
	80	0.12	-0.38	-0.38	0.50	0.50	0.00
	90	-1.20	-1.57	-1.58	0.37	0.38	-0.01
	104	-1.08	-1.38	-1.41	0.30	0.33	-0.03
	160	-0.36	-0.44	-0.45	0.08	0.09	-0.01
	188	0.00	0.00	0.00	0.00	0.00	0.00
5	6	0.00	0.00	0.00	0.00	0.00	0.00
	80	0.24	-0.24	-0.24	0.48	0.48	0.00
	90	-1.08	-1.46	-1.48	0.38	0.40	-0.02
	104	-1.92	-2.17	-2.20	0.25	0.28	-0.03
	160	-1.08	-1.34	-1.35	0.26	0.27	-0.01
	188	0.00	0.00	0.00	0.00	0.00	0.00
6	6	0.00	0.00	0.00	0.00	0.00	0.00
	80	0.24	-0.07	-0.08	0.31	0.32	-0.01
	90	-0.48	-0.54	-0.55	0.06	0.07	-0.01
	104	-1.08	-1.33	-1.34	0.25	0.26	-0.01
	160	-1.44	-1.70	-1.69	0.26	0.25	0.01
	188	0.00	0.00	0.00	0.00	0.00	0.00

a) Difference = Measured - Calculated

b) Difference = 3D - 2D

Note: Max difference is underlined